MASTER

Giant magnetoresistance in magnetic multilayers grown on grooved substrates

van Zon, A.M.A.

Award date:
1996

Giant Magnetoresistance in magnetic multilayers grown on grooved substrates

A.M.A. van Zon

October 1996

Abstract.

In this research, the GMR-effect in Co/Cu, Co/Ru, Fe/Cr and Fe/V magnetic multilayers grown at an angle onto grooved substrates is investigated. The GMR-effect is measured in both CIP (Current In Plane) and CPP (Current Perpendicular to Plane) configuration. The results are analysed using a two channel model derived form the Boltzmann Transport Equation. The GMR-effect in the Co/Cu and Fe/Cr multilayers is about ten times higher compared to the GMR-effect in the Co/Ru and Fe/V multilayers. In the latter two systems, a magnetic dead layer is present on the interface between the magnetic and nonmagnetic layers, leading to a decrease in the GMR-effect.

Technology assessment.

An important technological application of magnetic materials is their use in magnetic recording equipment. A few examples are a magnetic recording strip on a credit card, a hard disk of a computer and a video tape. Because there is a growing need for increased storage capacity, the size of the magnetic structures is reduced and magnetic sensors have to be more and more sensitive. Due to the rapid developments in thin film growing technologies in the 1980s, it became possible to grow multilayers consisting of thin films as thin as 10 Å and in 1988 the GMR-effect, the change of the resistance of a multilayer when a magnetic field was applied, was discovered. Soon after the discovery of the GMR-effect, it was recognised that this effect could be very promising for applications. A big advantage compared to the sensors based on the AMR-effect (the sensors now often used are based on this AMR-effect) is their high sensitivity. This means that a higher storage density can be used. Also memory chips based on the GMR-effect are of interest.

Several research labs in the world are now looking for a way to make very sensitive sensors suitable for use in magnetic recording equipment. Various samples of alternating stacks of thin films of certain materials are investigated, both theoretically and experimentally. Two examples are the so called spin-valves, containing three layers, and multilayers. Also various combinations of materials are examined for a better understanding of the GMR-effect.

Table of contents.

1. Introduction 1
1.1 Giant magnetoresistance. 1
1.2 The CIP- and CPP-configuration. 3
2. Theory 5
2.1 Impurity scattering 6
2.2 Transport in metallic multilayers 10
2.2.1 The Boltzmann model 11
2.2.2 The CIP configuration. 11
2.2.3 The CPP-configuration. 13
2.3 The influence of superlattice potential 16
2.4 Interlayer exchange coupling 19
3. Experimental set-up 20
3.1 Measuring in CPP-configuration. 20
3.2 Sample fabrication. 21
3.3 Sample characterisation. 23
3.3.1 VSM measurements 23
3.3.2 X-ray diffraction. 24
3.4 Magnetoresistance measurements. 25
4. Results and discussion. 27
4.1 Co/Cu multilayers. 27
4.2 Co/Ru multilayers. 28
4.3 Fe/V multilayers. 35
4.4 Fe/Cr multilayers. 38
5. Conclusions. 42
6. References. 43
7. Acknowledgements 45

1. Introduction

An important technological application of magnetic materials is their use in magnetic recording equipment like hard disks and DCC tape. Because there is a growing need for increased storage capacity, the size of the magnetic structures is reduced and magnetic sensors have to be more and more sensitive. Several research labs in the world are now looking for a way to make very sensitive sensors suitable for use in magnetic devices.

The type of sensor that is now often used in recording equipment is based on the AMR (Anisotropic MagnetoResistance). In these sensors the resistance changes as the angle between the current and the magnetisation of the sample is changed. This is called the AMR-effect and occurs only in ferromagnetic materials. The magnitude of the effect is about 5%.

Due to the rapid developments in thin film growing technologies in the 1980s, it became possible to grow multilayers consisting of thin films as thin as 10 Å. Studying the properties of these multilayers became a new direction in research and in 1986 the group of Peter Grünberg found that two magnetic layers separated by a nonmagnetic interlayer were magnetically coupled [1]. The coupling appeared to be either ferromagnetic or antiferromagnetic depending on the thickness of the nonmagnetic interlayer. Nowadays this coupling is called interlayer exchange coupling.

In 1988, the group of Albert Fert reported a change of about 100% in the resistance of Fe/Cr multilayers when a magnetic field was applied [2]. They explained the effect by spin dependent scattering and called it the Giant MagnetoResistance effect (GMR). This means that there is a difference in resistivity between spin up and spin down electrons. In the following years multilayers of different materials as Co-Cu and Ni/Fe-Co were examined leading to the same giant magnetoresistance effect.

All these experiments were done with MBE (Molecular Beam Epitaxy) grown multilayers. This reduced the practical applications due to the complicated system. In this research we examine the GMR-effect in e-beam evaporated multilayers in a high vacuum system. Apart from the well known magnetic multilayers Fe/Cr and Co/Cu, we examine the GMR-effect in Fe/V and Co/Ru multilayers.

1.1 Giant magnetoresistance.

In a simple description of the GMR-effect, the current is split in a spin up and a spin down channel. This is called the two channel model. In figure 1.1 the electron transport for both channels through the multilayer is shown.

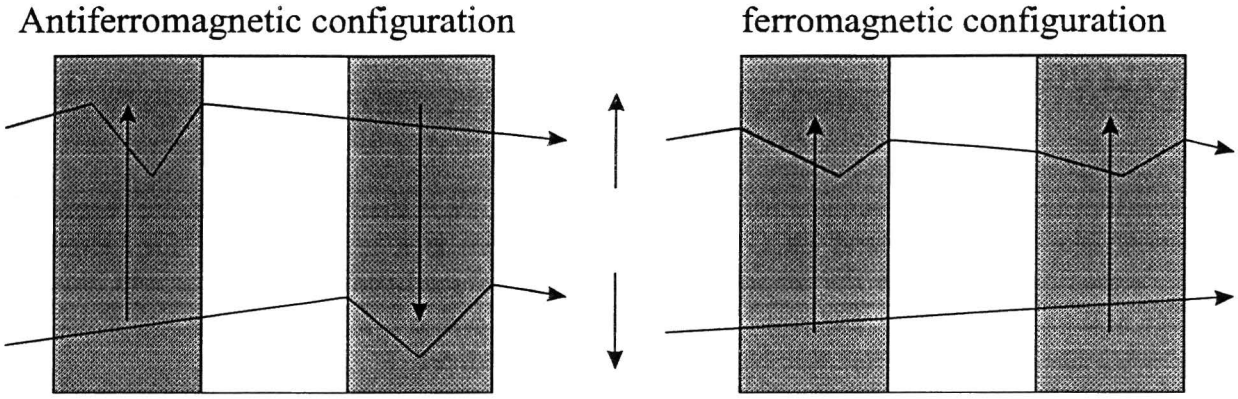

figure 1.1. *Schematic view of the electronic transport through a multilayer in the antiferromagnetic and ferromagnetic situation. The arrows indicate the magnetisation and spin direction.*

In this figure the multilayer is represented by two layers of ferromagnetic material (grey) separated by a nonmagnetic layer (white). In this example the minority spin electrons (spin- and magnetisation directions are opposite) have a higher resistivity than the majority spin electrons (spin- and magnetisation are parallel). In the antiferromagnetic situation the resistance of both spin channels is equal. The spin down electrons scatter mainly in the first magnetic layer where the spin up electrons scatter mainly in the second magnetic layer. In a magnetic field the magnetisation of both layers is parallel and the spin down electrons can move through the multilayer without scattering. This shunting effect causes a decrease in resistance leading to the GMR-effect. The two channel model can also be represented by a resistor scheme. For both the ferromagnetic and the antiferromagnetic situation it is shown in figure 1.2. The big blocks indicate a high resistance due to the strong scattering of the minority electrons.

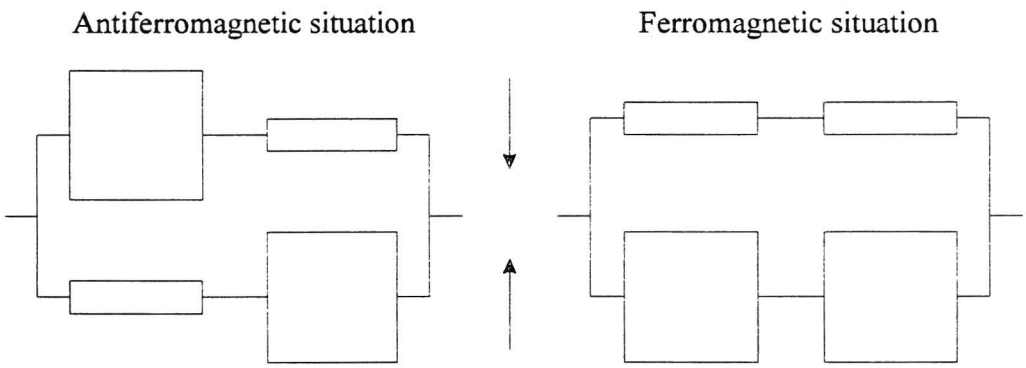

figure 1.2. *Resistor model of figure 2.1. The big blocks indicate a higher resistance.*

The spin dependent scattering processes can occur within the bulk of the magnetic layers but also at the interface between the magnetic and nonmagnetic layers. The scattering asymmetry, the ratio of spin up and spin down scattering, is a very important parameter in GMR. The process of spin dependent scattering will be described in chapter 2.

1.2 The CIP- and CPP-configuration.

Most of the GMR-measurements are done in the CIP (Current In Plane) configuration. In this configuration the current is parallel to the layers as shown in figure 1.3. Another geometry to measure the GMR-effect is the CPP (Current Perpendicular to Plane) configuration. In this configuration the electrons pass all the interfaces between magnetic and nonmagnetic layers. This interface scattering is thought to be very important in GMR and is optimally used in this configuration. Another advantage of the CPP-configuration is the more straightforward possibility to model the electronic transport. But, unlike the CIP- configuration, it is not easy to measure the resistances of the samples. The thickness of the multilayer is very small compared to the area perpendicular to the growth direction. This means when measuring the GMR, you have to deal with very low resistances.

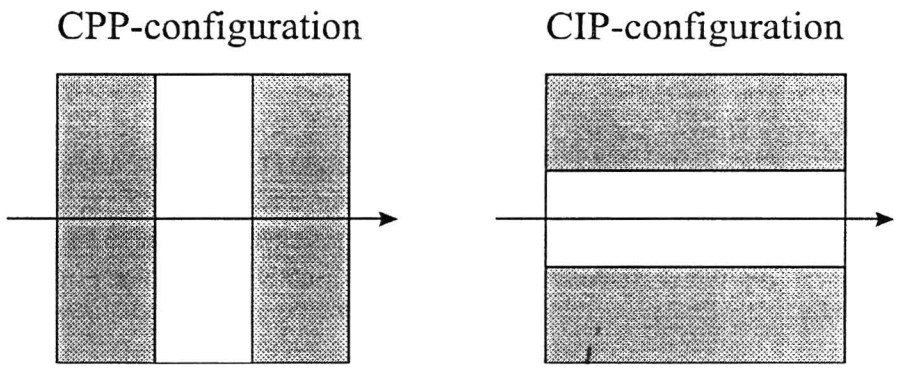

Figure 1.3. *Schematic view of the CPP (Current Perpendicular to Plane) and the CIP (Current In Plane) configuration.*

There are two possible solutions for solving this problem, either using very sensitive measuring equipment or enhancing the resistance by microstructuring. The first method was first investigated by a group at the Michigan State University [3]. The second method is used at the Philips research laboratories [4]. Both two methods will be discussed in chapter 3.

An alternative to microfabrication is to use grooved substrates. The substrate and multilayer are shown in figure 1.4. When the multilayer is deposited perpendicular to one of the grooves, separate multilayers are grown. When these multilayers are connected to each other, the total resistance of the multilayer is enhanced. The arrow in figure 1.4 indicates the ideal current path.

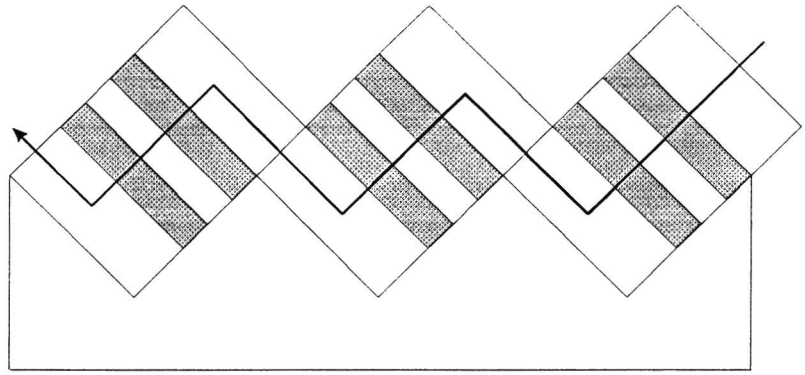

Figure 1.4. *Schematic view of a multilayer grown on a grooved substrate. The arrow indicates the ideal current path through the sample.*

In the separate pillars the current path is perpendicular to the plane of the multilayer. Now it is possible to measure the giant magnetoresistance in the CPP-configuration without sensitive measuring equipment and microfabrication. This technique is used in this research. Grooved substrates are also used by the group of Shinjo [5]. They used these grooved substrates for measuring the GMR-effect in the CAP (Current with Angle to Plane) configuration. This is an intermediate configuration between CIP and CPP. further description of the fabrication of the multilayers and the measuring of GMR-effect will be given in chapter 3. The results of the measurements will be given and discussed in chapter 4. Finally, in chapter 5, some conclusions will be drawn.

2. Theory.

To calculate the magnetoresistance of a multilayer, the bandstructure of the multilayer, as well as the scattering possibility for the electrons and the influence of the electric field on the electrons (transport) has to be known. Until now, a qualitatively correct theory including all these aspects is not yet developed. In this chapter we will describe the most important aspects of the GMR-effect. These aspects are shown in figure 2.1.

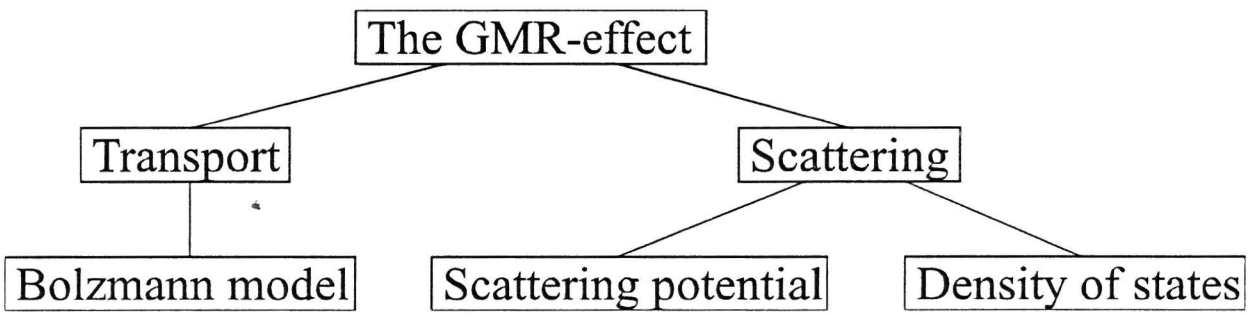

Figure 2.1. *The different aspect of the GMR-effect described in this chapter.*

In an isolated atom the electrons move in orbitals around the nucleus. Both angular momentum and electron spin contribute to the total magnetic moment of the atom. Each electronic state can be filled with two electrons, one with spin up and one with spin down. When a spin up and a spin down electron move in the same orbital, their wavefunctions have a large overlap and therefore the electrons feel a large Coulomb repulsion. For some atoms the energy can be reduced by changing an electron from spin and move it to another (higher) orbital. The overlap between the wavefunctions, and therefore the Coulomb repulsion, is decreased. When the energy difference between the two orbitals is smaller then the energy difference caused by the Coulomb repulsion, the situation of two parallel spin has less energy and the atom has a magnetic moment. The magnetic moment of an isolated atom can be calculated using the Hund's rules of which the first rule is described above.

In metallic solid state materials, the electronic states are changed due to the interaction with neighbouring atoms (quenching of the orbitals) and, as a result, the angular momentum in the direction of the magnetic field is averaged to zero [6]. Therefore the angular momentum of the electrons do no longer contribute to the magnetic moment of the atoms. The magnetic moment (in μ_b) is just the difference in the number of spin up and spin down electrons. When there is a difference in the number of spin up and spin down electrons and all these spins are aligned, the metal is ferromagnetic or antiferromagnetic depending on the alignment (parallel or antiparallel).

When an impurity atom is present in a metal host, the conduction electrons can scatter on the impurity. In a multilayer, the impurity can be a lattice impurity located in the bulk of the layers or an impurity caused by interface roughness. If the metal host, or the impurity (or both) is

magnetic, the scattering can be spin dependent. In a magnetic multilayers this spin dependent scattering leads to the GMR-effect.

2.1 Impurity scattering.

The resistivity of a metal depends on the mean free path of the conduction electrons in the metal, which is described by the Drude formula. The mean free path depends on the number of the scattering sources and the scattering possibility. To describe the scattering possibility ($W_{k,k'}$) of an electron with an impurity, Fermi's golden rule can be used, which is:

$$W_{k,k'} = \frac{2\pi}{\mathrm{h}} \left| \langle k' | V_{imp} | k \rangle \right|^2 \delta(E_F - E_{k'}) \qquad (2\text{-}1)$$

Here V_{imp} is the scattering potential caused by the impurity. $\delta(E_f - E_{k'})$ limits scattering to electrons at the Fermi surface. The scattering chance $W_{k,k'}$ does not give the actual scattering rate. In order to calculate the actual scattering rate the electron density of states at the Fermi level has to be considered. This density of states gives the possible states for an electron to scatter into. Electron scattering is enhanced by a large density if states at the Fermi level. This density of states is different for each metal as is shown in figure 2.2.

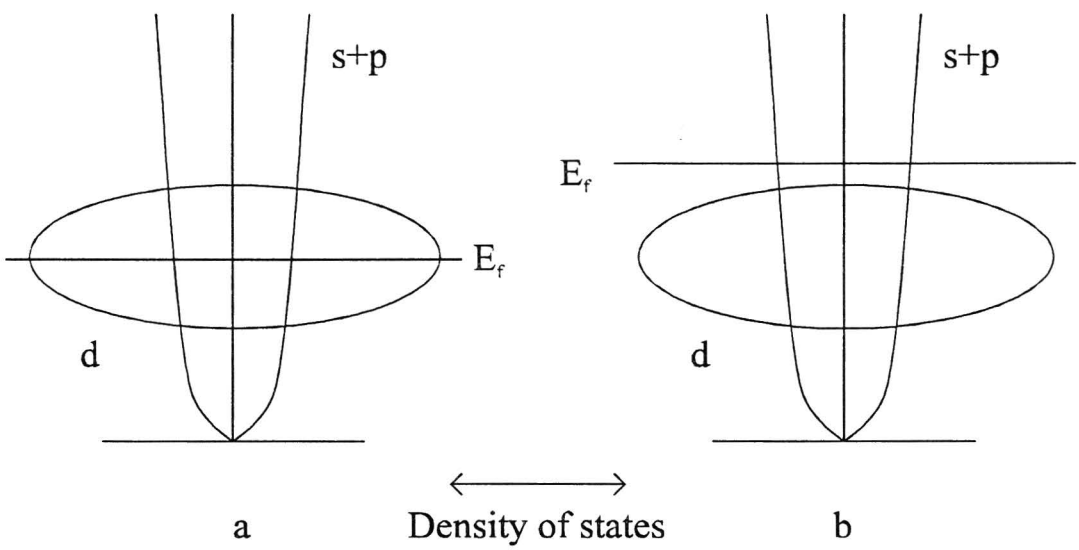

Figure 2.2. *Density of states of two different materials. The d and s+p bands are shown.*

In figure 2.2a the Fermi level is approximately halfway the d-band as is the case for transition metals like V, Cr and Ru. The density of states in figure 2.2b is above the top of the d-band. The d-band is completely filled like in Cu and Al. In this case there are fewer possible states for the electrons to scatter into. For magnetic metals there's a difference in density of states between spin up and spin down electrons. In, for example Co, the majority spin d-band is

completely filled while the minority d-band is approximately half filled. Minority electrons, therefore, have higher scattering rate.

Another way to describe the scattering of a conduction electron at an impurity is to look at the wavefunctions of the conduction electrons in the presence of a scattering potential. This is interesting because scattering can than be related to the number of d-electrons a possible impurity. In the following part we consider free electrons and a centro symmetric scattering potential with size R. The actual shape of the scattering potential is not very important. At a distance r>>R the solution of the Schrödinger equation for free electrons in the presence of a scattering potential can be found in several textbooks [7] and is:

$$\psi_{k,l} = e^{ikr} + \left[\sum_l (2l+1)\frac{S_l(k)-1}{2ik}P_l(\cos\theta)\right]\frac{e^{ikr}}{r} \qquad (2\text{-}2)$$

with $P_l(\cos\theta)$ the Legendre polynomial of order l. $S_l(k)=e^{2i\delta(k)}$ where δ_l is the faceshift between incoming and outgoing waves. The second term on the right hand side describes electrons scattered by the impurity. Due to the scattering potential, the number of electrons close to the potential is changed (the virtual bound state). This change in number of electrons is the difference, Z, in number of electrons between the host and the impurity atom. This difference can be calculated by integrating the second term of equation (2.2) over a volume, large enough compared to the volume of the scattering potential. In this way the Friedel sum rule [8] is derived, which is:

$$Z = \frac{2}{\pi}\sum_l (2l+1)\delta_l \qquad (2\text{-}3)$$

The scattering can now be described by the scattering cross section σ. This scattering cross section is closely related to the electron flux caused by the scattering potential. This is related to the second term on the right hand side of equation (2.2). The total cross section is found to be:

$$\sigma = \frac{4\pi}{k^2}\sum_l (2l+1)\sin^2\delta_l(k) \qquad (2\text{-}4)$$

For transition metal impurities in a metal host the main scattering is due to a different number of d-electrons, This means that in equation (2.4) only the l=2 term is nonzero. Then with $z = n_d^{host} - n_d^{imp}$ equation (3) becomes:

$$\sigma \sim \sin^2\left[\frac{\pi}{10}(n_d^{host} - n_d^{imp})\right] \qquad (2\text{-}5)$$

with n_d the number of d-electrons of the atom. For magnetic impurities with spin dependent scattering, equation (5) has to be considered per spin direction. When there's no difference between the number of d-electrons of host and impurity, the conduction electrons do not feel the impurity and therefore there is no scattering. When the difference is 10 electrons, the potential well is just deep enough for a bound d-state containing 10 d-electrons. In a more realistic metal the electrons will have different wave functions with different band structure and density of states. For example, impurities in Cr have a greater influence on the conductivity than impurities in Cu. This is caused by a difference in density of states at the Fermi level. But the relation between conductivity and type of impurity is well described by equation (2.5). For a magnetic impurity in a metallic host, its magnetic moment is the difference between spin up and spin down electrons (this because the angular momentum is zero and for virtual bound states the influence of the angular momentum is very little). Then it is clear that scattering is also dependent on the magnetic moment of the impurity. From the cross section in equation (2.5) one can calculate the associated scattering frequency $1/\tau$, which is:

$$\frac{1}{\tau} = n\sigma v_f \qquad (2\text{-}6)$$

in which n is the number of impurities and v_f the Fermi velocity. Using equation (2.5) and (2.6) we find for the spin asymmetry parameter $\alpha=\rho^{\uparrow}/\rho^{\downarrow}$:

$$\alpha = \frac{\sin^2(\frac{\pi}{5}[n_d^{\uparrow imp} - n_d^{\uparrow host}])}{\sin^2(\frac{\pi}{5}[n_d^{\downarrow imp} - n_d^{\downarrow host}])} \qquad (2\text{-}7)$$

This is an expression for the spin asymmetry parameter α for magnetic impurities in a free electron gas. From equation (2.7) it is clear that an optimum in α is reached when n_d^{imp}-n_d^{host}=0 for one spin channel. As an example, the number of d-electrons per spin channel is given for several materials in table 1 [9]. The total number of d-electrons per atom differ from the single atomic values due to hybridisation effects.

Table 2.1. *Number of d-electrons per spin channel for several materials.*

	$n^{\uparrow}$	$n^{\downarrow}$	$m(\mu_b)$	n_{tot}
Iron	4.6	2.4	2.2	7
Chromium	2.5	2.5	0	5
Vanadium	2	2	0	4
Cobalt	5	3.3	1.7	8.3
Copper	5	5	0	10
Ruthenium	3.5	3.5	0	7

multilayers which are well known for their spin dependent scattering are multilayers are Fe/Cr and Co/Cu. From table 2.1 it is clear that these combinations have great asymmetry in number of d-electrons. In Fe/Cr the number of minority spin electrons ($N^{\downarrow}$) is approximately equal,

where in Co/Cu it is the number of majority spin electrons ($N^{\uparrow}$) which is equal. Other combinations like Fe/V and Co/Ru have also great asymmetry in number of d-electrons. It is known from experiments that V impurities in Fe as well as Ru impurities in Co scatter spin dependent [11] [12]. Because a large asymmetry in spin dependent scattering is important for a large GMR-effect it is interesting to investigate the GMR-effect in Fe/V and Co/Ru multilayers.

The number of d-electrons in table 2.1. are bulk the values. In a multilayer these values could change because atoms located at the interface have other neighbours. This could change the spin asymmetry with respect to bulk materials. Itoh et. al. [9] have calculated the magnetic moments of atoms located at Fe/TM and Co/TM multilayers. Calculations are done for ideal interfaces and interfaces with one magnetic atom in the nonmagnetic layer or vice versa. To calculate the GMR-effect they assumed that scattering is only caused by these interface impurities. Then the scattering potential can be derived and, with Fermi's golden rule and realistic density of states, the relaxation time. Finally the resistance and the GMR-effect is calculated with the Drude formula. The results of these calculations are shown in figure 2.2. The high GMR-effect in Fe/Cr and Co/Ru multilayers is can be understood by looking at the number of d-electrons given in table 2.1.

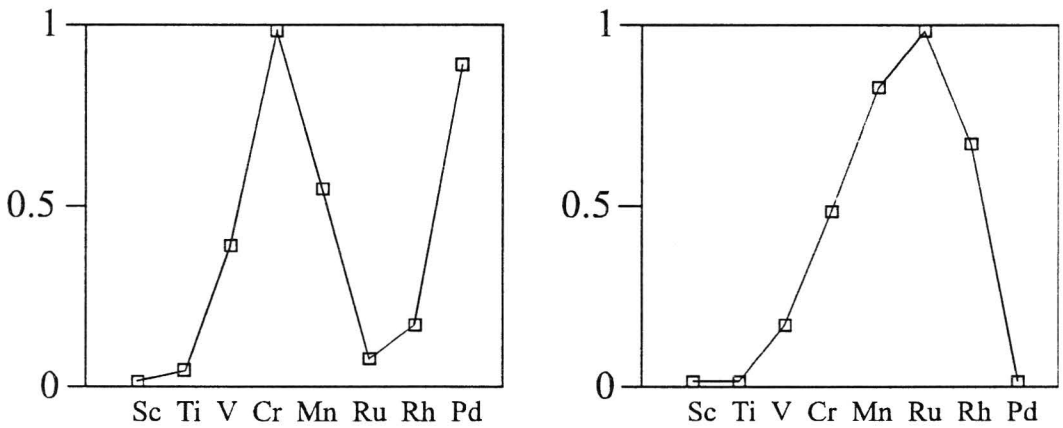

Figure 2.3. *GMR-effect of Co/TM and Fe/TM multilayers. Values are normalised to unity*

Because the scattering cross section σ is dependent on the number of d-electrons, it is important to know the behaviour of magnetic impurities on the interface between magnetic and nonmagnetic materials. Coehoorn [10] calculated the influence of interfacial structure on the magnetic moment of atoms located at the interface. He did his calculations for Fe/Cr and Fe/V multilayer systems. The interface varies from perfectly flat to totally interdiffused. The interdiffused region has a thickness of one atomic layer. Coehoorn concludes that there is a difference between the Fe/Cr and Fe/V interfaces in their dependence on the interfacial structure. In a Fe/Cr multilayer the Fe and Cr moments do not differ as a function of the interface structure. The reason for this is the antiferromagnetic (AF) coupling between Cr atoms and between Cr and Fe atoms. An example is given in figure 3.

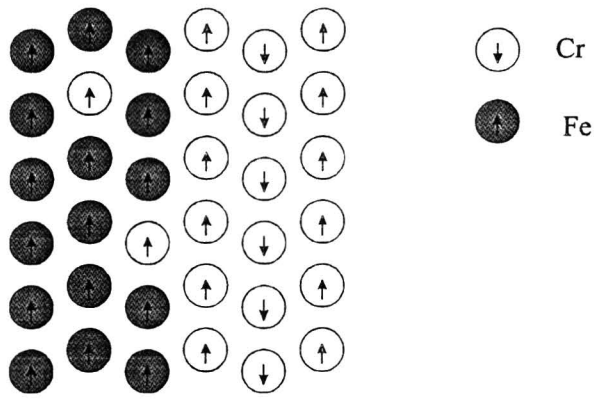

Figure 2.4. *Cr/Fe interface with an interface impurity and a bulk impurity*

The competing AF-coupling between the atoms suppresses the magnetic moment of the Cr interface impurity. For a Cr impurity in bulk Fe the AF-coupling between Cr atoms is absent (there are no Cr-neighbours). Therefore the moments of such an impurity is much higher. In contrast The V-V exchange interaction is very weak and therefore V interface impurities have much larger induced moments. The magnetic moments of Fe atoms located at the Fe/V interfaces are reduced. The magnetic moment of the V atoms is approximately linear with the number of Fe neighbours and the change in the magnetic moment of Fe impurities is approximately linear with the number of V atoms. In Fe/V multilayers interface roughness leads to a decrease of the total magnetic moment of the multilayer. The reduced Fe and increased V moments change the asymmetry to a lower value compared with the values of table 2.1.

2.2 Transport in metallic multilayers

Electronic transport has, in the past, been described by several models. The most transparent approach is based in the Boltzmann Transport Equation (BTE). In this approach an distribution function f(**k**) is introduced to describe the distribution of the electrons. This distribution is changed due to the electric field and scattering of the electrons at impurities. In order to calculate the transport of conduction electrons in a metal, realistic density of states and all scattering chances $W_{k,k'}$ have to be used. Even when all these values are known, it is very difficult to calculate the resistance of a metal. A useful approximation is the so called relaxation time approximation. It says that after every scattering, the electrons are scattered to the equilibrium distribution, the Fermi-Dirac distribution. Within this approximation the electric field causes a displacement of the Fermi sphere resulting in a net current in the direction of the electric field. The displacement is depending on the strength of the electric field and the mean free path of the conduction electrons.

In a metallic multilayer, the mean free path, and also the electric field can be different in the different layers. The current can no longer be expressed as a displacement of the Fermi sphere.

It is useful to construct localised electrons with wavepackets. The construction of localised electrons is limited due to the uncertainty principle $\delta\mathbf{x}\delta\mathbf{k}\sim h$. The distribution of electrons can then be expressed as f(**x**,**v**). In this chapter transport in metallic multilayers is described using the BTE and the distribution function f(**x**,**v**). The differences between the CIP- and the CPP-configuration are explained. The GMR-effect can also be described within the Kubo-formalism. Within this approach several calculations are done to calculate transport in layered systems [24] [25].

2.2.1 The Boltzmann model.

The BTE is derived from conservation of the distribution if we follow a volume element **drdv** along a flowline. Thus, in steady state, we obtain:

$$\frac{df}{dt} = \left(\frac{df}{dt}\right)_{\vec{E}} - \left(\frac{df}{dt}\right)_{scat} = 0 \qquad (2\text{-}8)$$

in which the first term describes the acceleration of the electrons in an electric field and the second term describes the scattering of the conduction electrons at impurities. This equation can be written as:

$$v \cdot \nabla_r f + a \cdot \nabla_v f = \left(\frac{df}{dt}\right)_{scat} \qquad (2\text{-}9)$$

where $\boldsymbol{v}$ and $\boldsymbol{a}$ is the velocity and the acceleration of the electrons respectively. Using the relaxation time approximation, the right hand side of equation 2.9 can be written as:

$$\left(\frac{df}{dt}\right)_{scat} = \frac{(f - f^0)}{\tau} = \frac{g}{\tau} \qquad (2\text{-}10)$$

where f^0 is the Fermi-Dirac distribution, g the deviation from the equilibrium and τ the relaxation time. In the CPP configuration spin-flip scattering is included. This leads to a similar type of scattering only with relaxation time τ_{sf}.

2.2.2 The CIP configuration.

In 1989, Camley and Barnas [13] proposed a theory of the GMR-effect based on the BTE. In our description we use diffuse boundary conditions for all electrons. The reflection caused by a potential step is neglected. In the CIP-configuration and keeping only linear terms in perturbation, equation (2.9) becomes:

$$\frac{\partial g}{\partial z}+\frac{g}{v_z\tau}=\frac{eE}{mv_z}\frac{df^0}{dv_x} \tag{2-11}$$

Spin-flip scattering is neglected. In bulk samples *dg/dz=0* and we obtain the Drude formula for conductivity. To calculate the GMR-effect, g is divided into separate terms for each layer (A/B/...), spin direction (↑/↓) and electrons moving to the right or left (+/-). The solution for $g_{A+\uparrow}$ becomes:

$$g_{A+\uparrow}=\frac{eE\tau}{m}\left[1+A_{+\uparrow}\exp\left(\frac{z}{\tau|z|}\right)\right] \tag{2-12}$$

The coefficients $A_{+\uparrow}$ and similar coefficients are unknown parameters which are to be determined through boundary conditions. When an electron reaches the interface it has a transition probability T. The other part (1-T) scatters diffuse. These two possibilities are shown schematically in figure 2.5. In this figure three layers (A,B,C) are shown.

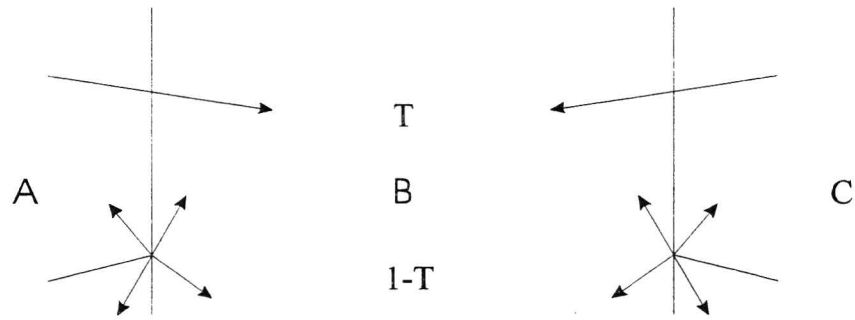

Figure 2.5. *Schematic view of interface transmission and interface scattering. A,B and C refere to three different layers in the multilayer.*

In layer B, next to the interface with layer A, the electrons with positive velocity that contribute to g, can only come from layer A, Thus,

$$g_{A+\uparrow}(z=\text{int})=Tg_{B+\uparrow}(z=\text{int}) \tag{2-13}$$

where T is the transmission coefficient of electrons going through the interface without scattering. The part that scatters (1-T) does not contribute to $g_{B+\uparrow}$. Having found all the various g's, we can find the current density in the direction of the electric field using

$$J(z)=\int v_x g(v_z,z)d^3v \tag{2-14}$$

The integration is done over the Fermi surface. The current in the entire structure is then found by integrating J(z) over the co-ordinate z. When T=0, all the electrons scatter at the interface. This means that the multilayer can be split in separate layers. In these separate layers there is

no GMR-effect. This means that the GMR vanishes when T→0. The same happens when the mean free path λ becomes smaller then the layerthickness of the nonmagnetic layer.. the three parameters t,T and λ are, together with the spin asymmetry parameter α, of great importance in the CIP-configuration.

2.2.3 The CPP-configuration.

In the CPP configuration, the current is perpendicular to the layers and therefore there is always a net transport of electrons through each interface. First consider an interface of two semi-infinite ferromagnetic materials (L and R) with opposite magnetisation. This situation is shown in figure 2.6. Far from the interface the current is spin polarised. In ferromagnet L, the spin up electron flux is larger than the spin down electron flux. In ferromagnet R, the spin down electron flux is larger than the spin up electron flux. This results in an accumulation of spin up electrons and a raise of the spin up chemical potential around the interface. The equilibrium is restored because electrons can change from spin direction via spin-flip scattering. Spin-flip scattering is, for instance, caused by electron magnon scattering or by scattering at paramagnetic impurities in a nonmagnetic layer [14].

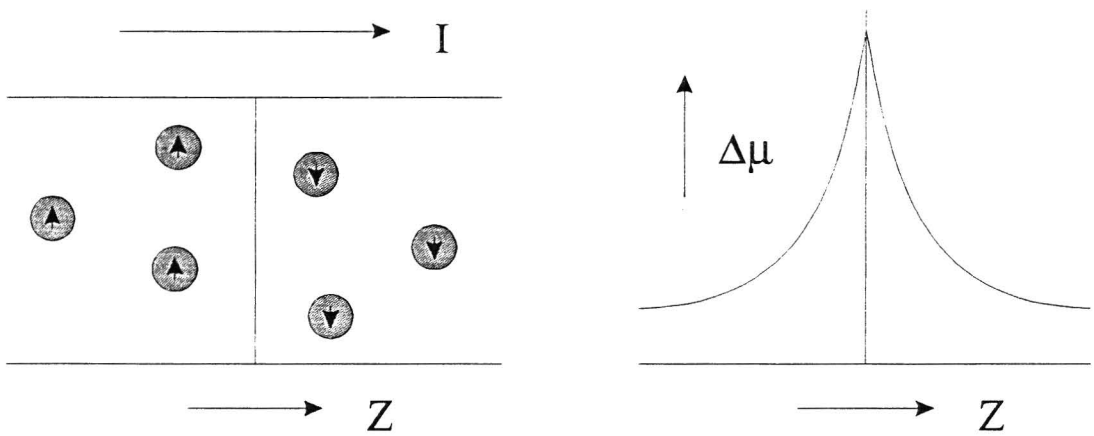

Figure 2.6. *Spin accumulation caused by a net transport of electrons through the interface. $\Delta\mu$ is the change in chemical potential caused by spin accumulation.*

Valet and Fert [15] calculated the resistance in the CPP-configuration including spin accumulation and spin-flip scattering. To account for spin accumulation they introduce a spin and position dependent chemical potential $\mu_s(z)$. For small perturbations, the distribution function f(z,**v**) can be written as:

$$f_s(z,v) = f^0(v) + \frac{df^0}{d\varepsilon}\{[\mu^0 - \mu_s(z)] + g_s(z,v)\} \qquad (2\text{-}15)$$

where μ^0 is the equilibrium chemical potential. By introducing equation (2.15) in the BTE, and keeping only linear terms in perturbation, we obtain:

$$v_z \frac{\partial g_s}{\partial z} + \left(\frac{1}{\tau_s} + \frac{1}{\tau_{sf}} \right) g_s(z,v) = v_z \frac{\partial \overline{\mu}_s}{\partial z}(z) + \frac{\overline{\mu}_s(z) - \overline{\mu}_{-s}(z)}{\tau_{sf}} \tag{2-16}$$

where $\mu_s(z)=\mu_s(z)-eV(z)$ is the electrochemical potential for spin s. τ_s and τ_{sf} are the relaxation times for spin conserved and spin-flip scattering respectively. The second term on the right hand side describes the relaxation to the equilibrium chemical potential through spin flip scattering. The other terms are also present in equation (2.11) for transport in the CIP-configuration. In the limit $\tau_s << \tau_{sf}$, The time between two scatter events is much smaller than the time between spin-flip scattering. equation (2.16) reduces to two simple macroscopic equations, which are:

$$\frac{e}{\sigma_s} \frac{\partial J_s}{\partial z} = \frac{\overline{\mu}_s - \overline{\mu}_{-s}}{l_s^2} \tag{2-17}$$

$$J_s = \frac{\sigma_s}{e} \frac{\partial \overline{\mu}_s}{\partial z} \tag{2-18}$$

Equation (2.17) expresses that the spin accumulation $\partial J_s/\partial z$ is balanced by spin flip scattering with spin-flip diffusion length l_s.. Equation (2.18) is Ohm's law with an effective electric field including spin accumulation. Obviously, proper boundary conditions have to be taken into account. These are the continuity of J per spin channel and the potential drop caused by localised interface scattering. With equations (2.17) , (2.18) and the boundary conditions, the total resistance of a multilayer can be calculated. These calculations lead to:

$$R^{(AP,P)} = M((1-\beta^2)\rho_f^* t_f + \rho_n t_n + 2(1-\gamma^2) r_b^* + 2r_{si}^{P,AP} \tag{2-19}$$

with R the total resistance per unit area, M the number of bilayers and

$$2r_b^* = r_{\uparrow(\downarrow)} \cdot \frac{1}{1-(+)\gamma}, 2\rho_f^* = \rho_{\uparrow(\downarrow)} \cdot \frac{1}{1-(+)\beta} \tag{2-20}$$

where $r_{\uparrow(\downarrow)}$ and $\rho_{\uparrow(\downarrow)}$ are interface and bulk resistance for the spin up (down) channel respectively. ρ_n is the resistance of the nonmagnetic layers. t_n and t_f are the layerthickness for the nonmagnetic and ferromagnetic layers and β and γ the bulk and interface spin asymmetry parameters. $r_{si}^{(P,AP)}$ is the spin-coupled interface resistance and is given by:

$$r_{si}^P = \frac{\frac{(\beta-\gamma)^2}{\rho_n l_{sf}^n} \coth\left(\frac{t_n}{2l_{sf}^n}\right) + \frac{\gamma^2}{\rho_f^* l_{sf}^f} \coth\left(\frac{t_f}{2l_{sf}^f}\right) + \frac{\beta^2}{r_b^*}}{\frac{1}{\rho_n l_{sf}^n} \coth\left(\frac{t_n}{2l_{sf}^n}\right) \frac{1}{\rho_f^* l_{sf}^f} \coth\left(\frac{t_f}{2l_{sf}^f}\right) + \frac{1}{r_b^*}\left[\frac{1}{\rho_n l_{sf}^n} \coth\left(\frac{t_n}{2l_{sf}^n}\right) + \frac{1}{\rho_f^* l_{sf}^f} \coth\left(\frac{t_f}{2l_{sf}^f}\right)\right]} \tag{2-21}$$

and

$$r_{si}^{AP} = \frac{\frac{(\beta-\gamma)^2}{\rho_n l_{sf}^n}\tanh\left(\frac{t_n}{2l_{sf}^n}\right) + \frac{\gamma^2}{\rho_f^* l_{sf}^f}\coth\left(\frac{t_f}{2l_{sf}^f}\right) + \frac{\beta^2}{r_b^*}}{\frac{1}{\rho_n l_{sf}^n}\tanh\left(\frac{t_n}{2l_{sf}^n}\right)\frac{1}{\rho_f^* l_{sf}^f}\coth\left(\frac{t_f}{2l_{sf}^f}\right) + \frac{1}{r_b^*}\left[\frac{1}{\rho_n l_{sf}^n}\tanh\left(\frac{t_n}{2l_{sf}^n}\right) + \frac{1}{\rho_f^* l_{sf}^f}\coth\left(\frac{t_f}{2l_{sf}^f}\right)\right]} \qquad (2\text{-}22)$$

Where $l_{sf}^{-2} = l_s^{-2} + l_{-s}^{-2}$. In the limit $t >> l_{sf}$, r_{si}^{AP} becomes equal to r_{si}^{P} and the GMR vanishes. Thus, the spin flip diffusion length is an important parameter in the CPP configuration where in the CIP-configuration the mean free path is the limiting parameter. This is a very important difference between both configurations.

In the limit $l_{sf} >> t$ the accumulation is no longer a function of z (there's not enough room for relaxation) and equations (2.19) turns into the same equation that can be derived from a simple resistor model, with for each spin channel different resistances. This is a very important result, which will show to be very useful in determining several spin dependent parameters of the multilayers. A schematic view of this resistor model is shown in figure 2.7.

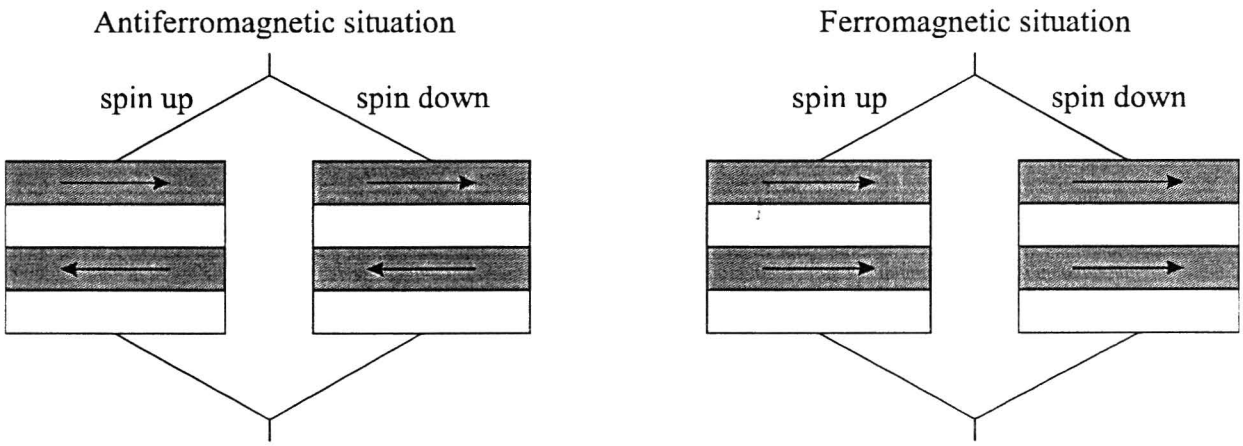

Figure 2.7. *Resistor model of the CPP-configuration. The rectangles indicate the separate layers in the multilayer (grey is magnetic). The two channels indicate the spin up and spin down channel. Both parallel and antiparallel configuration is shown.*

Now, the current is split in two separate parts for spin up and spin down electrons. The resistance of one spin channel, for example the spin up channel, is then found by adding up the resistances of each layers and interfaces. In the antiferromagnetic configuration, the resistance of the spin up channel can be separated in the following terms:

$$R^{+}_{(AF)} = r^{\uparrow}_{\text{int}} + \frac{\rho^{\uparrow}_f t_f}{A} + r^{\uparrow}_{\text{int}} + \frac{\rho_n t_n}{A} + r^{\downarrow}_{\text{int}} + \frac{\rho^{\downarrow}_f t_f}{A} + r^{\downarrow}_{\text{int}} + \ldots. \qquad (2\text{-}23)$$

A similar expression can be found for the spin down channel and for the ferromagnetic configuration. With these expressions the GMR can be calculated. Then, for a multilayer with total length L and M bilayers, we find the expression:

$$\sqrt{(R^{(AP)} - R^{(P)})R^{(AP)}} = \beta \frac{t_f}{t_f + t_n} \rho^*_f L + 2\gamma r^*_b M \qquad (2\text{-}24)$$

As an illustration, in figure (2.8) we plot $\sqrt{(R^{(AP)} - R^{(P)})R^{AP)}}$ as a function of the nonmagnetic layerthickness t_n for a multilayer with fixed total thickness L. These plots are calculated with infinite spin-flip diffusion length and with a spin-flip diffusion length of 200Å.

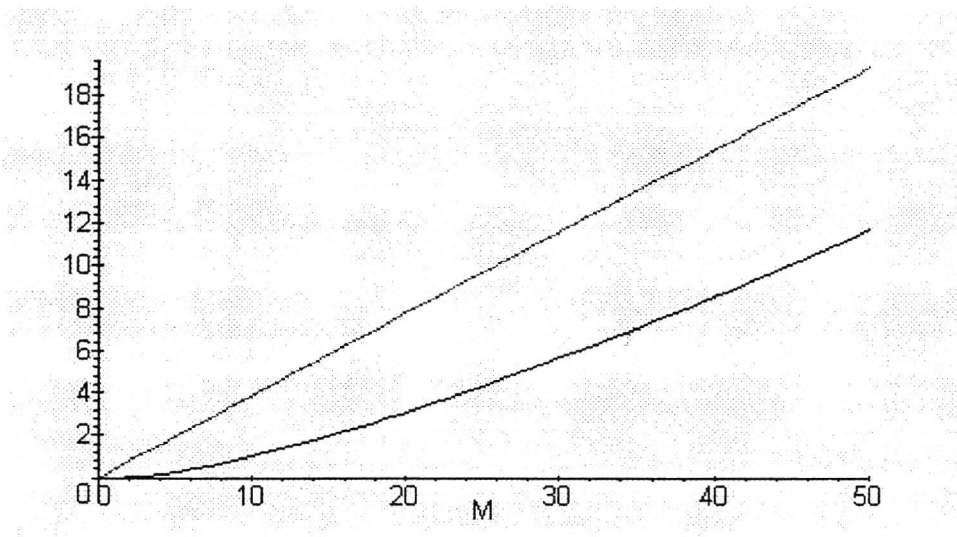

Figure 2.8. *$\sqrt{(R^{(AP)} - R^{(P)})R^{AP)}}$ as a function of the number of bilayers for a multilayer of fixed total length L.*

2.3 The influence of superlattice potential

In multilayers, the electrons feel a different potential with respect to bulk crystals. This difference is caused by the different materials in the multilayer. The potential landscape of the multilayer is referred to as the superlattice potential. In paragraph 2.2 transport through multilayers is described. In these models, based on the BTE, the influence of the superlattice potential was excluded. all interface scattering is assumed to be diffuse. In this paragraph we

explain the influence of superlattice potential in ballistic transport, where diffuse scattering is absent, and extend this to the diffuse transport regime.

Consider two electrodes separated by an insulating barrier and only connected via a small opening in the barrier. When the diameter of the opening is much smaller than the mean free path and much greater than the electron wavelength, such a structure is referred to as a ballistic point contact. The conductance of such a point contact is finite due to its finite cross section. The conductance now only depends on the projection of the Fermi surface in the direction of the current [16]. The conductance is:

$$G(n) = \frac{e^2}{h}\frac{A}{4\pi^2}\frac{1}{2}\sum_{vs} S_{vs}(n) \qquad (2\text{-}25)$$

where A is the cross section of the point contact, ν the band index, s the spin index and $S_{vs}(n)$ the projection of the Fermi surface in the direction n. For a free electron gas the Fermi surface is a closed sphere and the projection are two circles with radius k_f. By substitution of $S(n)=2\pi k_f^2$ in equation (2.25) the free electron expression for ballistic conductance is obtained. This conductance is isotropic as expected for a free electron gas.

In a multilayer the electrons feel a different potential in the magnetic and the nonmagnetic layers. This difference is depending on the materials used in the multilayer. This total potential of the multilayer can be described with a Kronig-Penney potential. In figure 2.9 the potential landscape for spin up and spin down electrons is given in the ferromagnetic and antiferromagnetic configuration. In the antiferromagnetic configuration there is no difference between both spin channels.

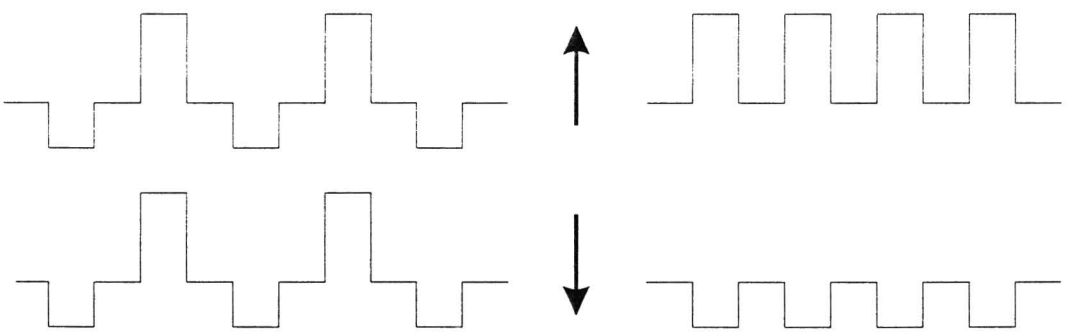

Figure 2.9. *potential landscape of the spin up and spin down electrons in the multilayer. Both ferromagnetic and antiferromagnetic configurations are shown.*

The electrons passing an interface (partly) reflect at the potential step. Total reflection is reached when the wavelength of the electrons perpendicular to the layers, $\lambda_\perp$, fits the multilayer thickness (Bragg reflection). The part of the electrons which is reflected does not contribute to the conductance. The projection of the Fermi surface is changed due to the potential landscape which is shown in figure 2.10. The positions of the gaps in the perturbed Fermi surface (white rings in figure b) correspond to the wavevectors of the Bragg reflection. These gaps refer to

electrons which are reflected totally. The size of the gaps is depending on the height of the potential step.

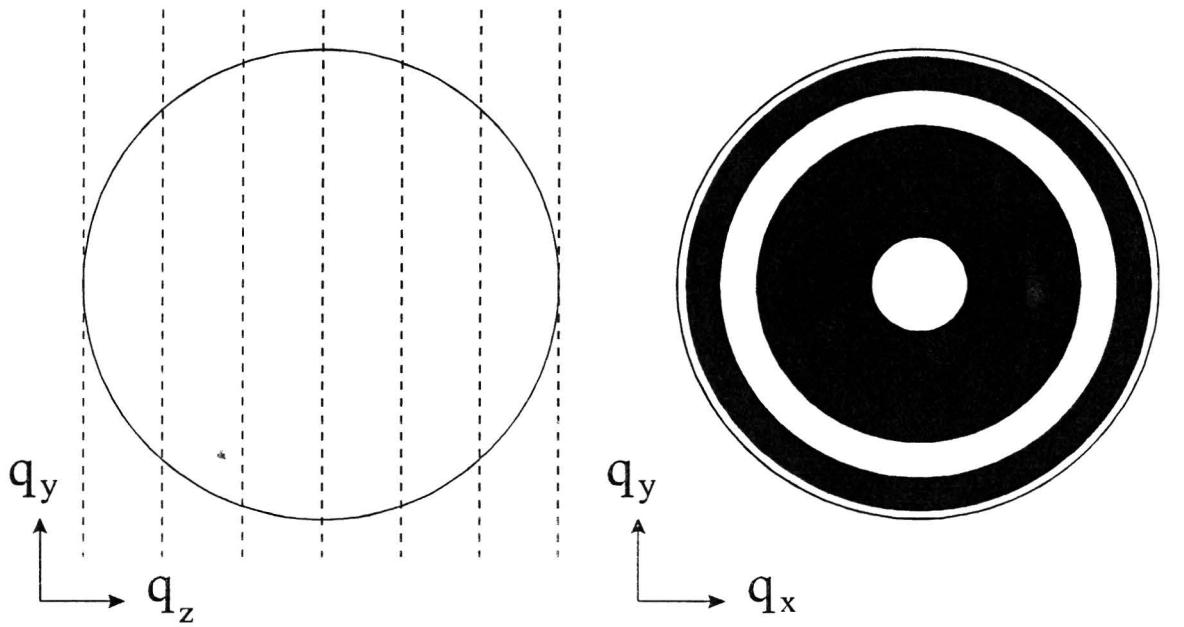

Figure 2.10. *(a) The cross section of the Fermi sphere at $q_x=0$. The dashed lines represent the wavevectors q_z for which Bragg reflection occurs. (b) The projection of the perturbed Fermi surface in the z-direction.*

In the CIP-configuration there are no potential steps in the direction of the current and consequently no Bragg reflection and gaps in the projection of the Fermi surface. In the CPP-configuration this is the case. Schep et. al. calculated the GMR in the ballistic regime in both the CPP- and the CIP-configuration [16]. They find, for instance, a CPP-GMR of 40% and a CIP-GMR of only 4% for Co-Cu multilayers containing three monolayers of atoms per layer.

The size of the Fermi surface is also important in the diffuse transport regime. In for example the Boltzmann model, the current is calculated by integrating the change in distribution g over all electrons contributing to the current, the Fermi surface. Gaps due to the superlattice potential lead to a change in the conduction. But this is not the only way that the Fermi-surface has an influence on the conductance. In the expression for the relaxation time τ, the density of states at the Fermi level is important. This density of states is just the sum of all possible $\mathbf{k}_f$'s. Gaps in the Fermi surface decrease the possibilities for an electron to scatter. Taking this into account, Zhang et. al. [17] calculated the GMR in both CIP and CPP configuration. They calculated the wavefunctions for a Kronig-Penney potential and used them to calculate the density of states and the global conductivity. The calculations are done in the limit where the mean free path is much larger than the multilayer thickness. They find a strong increase in GMR when the height of the potential step in increased.

Recently, Mathon [26] calculated that the GMR-effect can be increased when the layerthickness of the separate layers is fluctuated (pseudorandom multilayers). He calculated that the CPP-GMR increases approximately exponentially with the number of bilayers due to

the so called Anderson localisation. A value of approximately 10^4 % is found in the CPP-configuration with a multilayer containing 50 bilayers.

2.4 Interlayer exchange coupling

Interlayer exchange coupling is a magnetic interaction between two magnetic layers separated by a nonmagnetic layer. This interaction is caused, like GMR in the ballistic regime, by spin dependent reflection of the conduction electrons at the interfaces in the multilayer. This mechanism can be understood qualitatively from the following simplified picture. A conduction electron, which can be represented by a plane wave with wavevector **k**, experiences a potential step at the interface between magnetic and nonmagnetic layer. Due to the potential step, part of the electron will be reflected where it interferes with the incoming wave leading to an oscillating wave in the nonmagnetic layer. The amplitude of the oscillating wave is related to the height of the potential step and the period is just $\pi/\mathbf{k}$. Because the potential step is different for spin up and spin down electrons the reflection coefficients and therefore the amplitudes of the oscillating waves are different. The result is a spin polarised wave in the nonmagnetic layer. The magnetisation of the second magnetic layer in now influenced by the spin polarised wave and thus by the first magnetic layer. A schematic view is shown in figure 2.11.

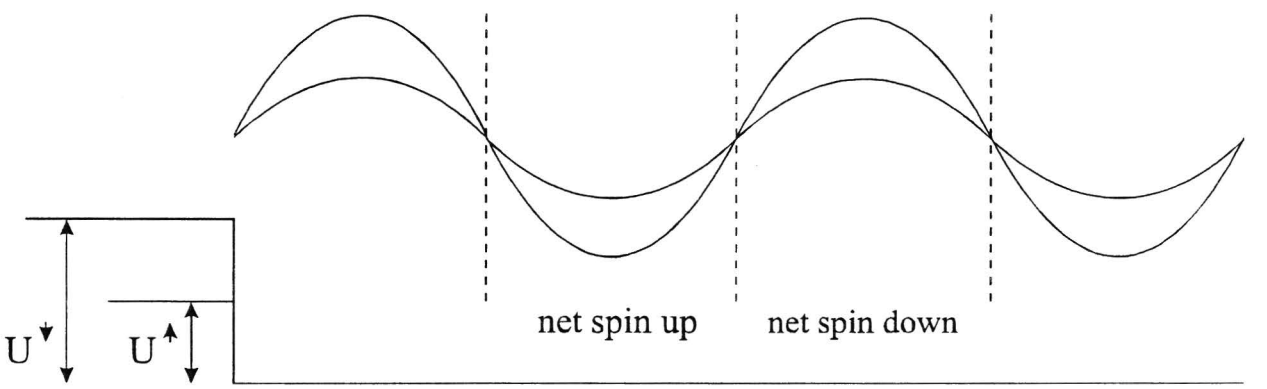

Figure 2.11. *Amplitudes of the oscillating waves caused by spin dependent reflection at the interfaces. The to potential steps $U^{\uparrow}$ and $U^{\downarrow}$ are shown.*

Bruno [18] calculated the total energy of the electron system for two magnetic layers A and B separated by a nonmagnetic layer with thickness D as a function of the angle θ between the two magnetic layers. He concludes that, apart from the D^{-2} decay, The strength of the coupling is determined by two factors: (i) The properties of the Fermi surface and (ii) the spin asymmetry of the reflection amplitude for the conduction electrons. The latter is also of great importance for GMR in the CPP-configuration. Therefore it is important to look at the results of the experiments done by Parkin [19]. He measured the coupling strength for all transition metal interlayers. He finds, for instance, a very strong coupling for Ru interlayers which indicates a great asymmetry in interface reflection in Co/Ru multilayers.

3. Experimental set-up

As already mentioned in the introduction, there are several methods to measure the GMR-effect in the CPP-configuration. In paragraph 3.1 we will first describe two important alternative methods for measuring the CPP-configuration. The fabrication of the samples grown on grooved substrates is described in paragraph 3.2. To characterise the actual structure of the multilayers magnetisation measurements and x-ray diffraction measurements are done. These are described in paragraph 3.3. Finally the set-up of the actual GMR measurements is given in paragraph 3.3.

3.1 Measuring in CPP-configuration.

The first solution of measuring in CPP-configuration was presented by the group of Michigan State University [3]. They used a very sensitive voltage measuring technique to measure the extremely small resistance. Such a technique, based on a sensitive SQUID (Superconducting QUantum Interference Device), is capable of measuring small resistances with nΩ resolution. Superconducting Nb strips are used for an uniform current distribution in the multilayer. The layers of the multilayer are in between these superconducting strips. The sample geometry is shown in figure 3.1.

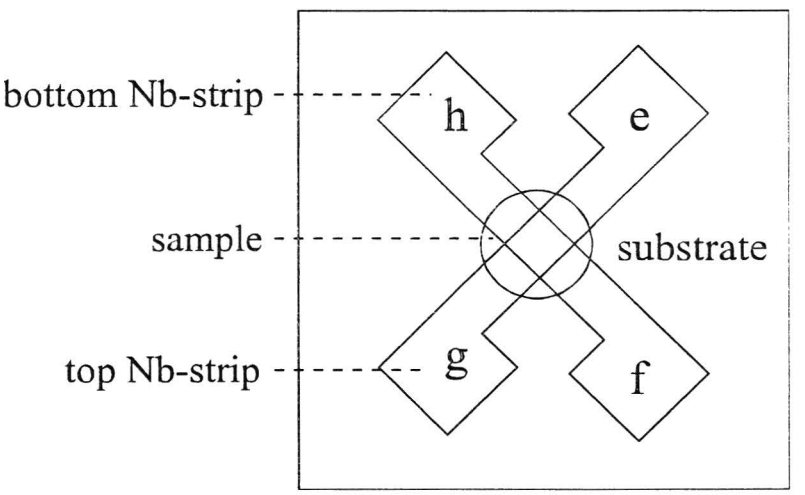

Figure 3.1. *Schematic view of the sample geometry used by the group of Michigan State University. e,f,g and h are contact leads.*

The superconducting Nb strips h-f and e-g are located at the top and the bottom of the multilayer respectively. e and h are contact strips and the voltage is measured between g and f. A disadvantage of using superconducting contacts is the limitation to measure only at to 4.2 K.

Another solution was found by the group at Philips research laboratories [4]. They fabricated microstructured pillars with a cross section ranging between 6 μm^2 to 130 μm^2 . Because of this small cross section they were able to measure GMR up to the room temperature. Now also the temperature dependence of GMR in the CPP-configuration could be investigated. Because of the difficulties involving microstructuring, making an analysis of the spin asymmetry parameters was impossible.

3.2 Sample fabrication.

In our technique we use a grooved substrate on which the multilayer is deposited. These substrates are based on semi-insulating nip. The fabrication of the grooved substrates is a standard process developed at Philips Research. This process is described by Van Gansewinkel [27]. The substrate with dimensions and the resulting multilayer is shown in figure 3.2.

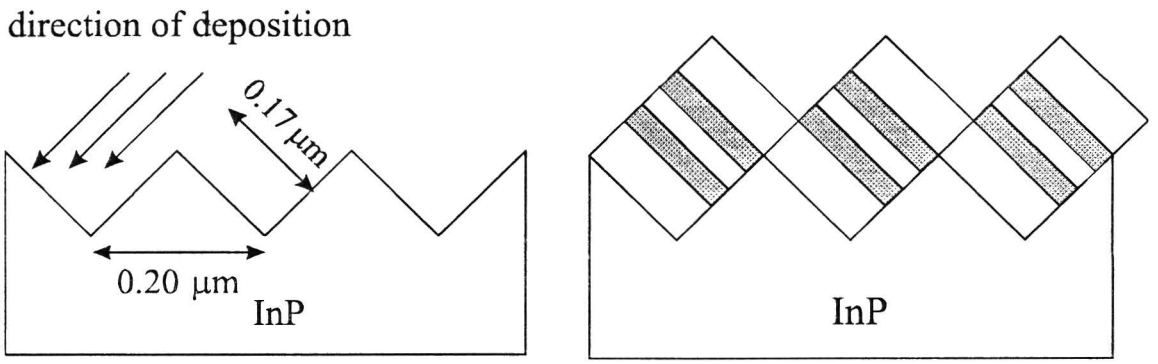

Figure 3.2. *A schematic view of a grooved substrate with dimensions. The arrows indicate the direction of the deposition. The result is shown in the right figure.*

The first samples in which grooved substrates were used have been grown in a MBE-system. The principle of MBE is to thermally evaporate a source and deposit the evaporated atoms on the substrate. All depositions are carried out at room temperature and at a pressure of 10^{-10} mbar. The typical growing rate is 0.1 Å/sec. Multilayers are also grown on grooved substrates using e-beam evaporation. In this technique an electron beam is focused on the material which has to be evaporated. The temperature of this material rises and as a result atoms leave the surface. The number of atoms leaving the surface is dependent on the temperature of the material and thus on the strength of the electronic beam. In this way the evaporation rate can be regulated in a range between 1 to 10 Ångstroms per second. The multilayers are evaporated at room temperature at a pressure of 10^{-7} mbar.

In the deposition process a 3 nm Cr layer is first deposited on the InP substrate to enhance the adhesion between the InP and the multilayer. Then the multilayer is deposited. The angle of deposition causes a pillar like growth. When the length of the separate pillars becomes larger than 0.17 μm the pillars are linked to each other. For an optimal CPP configuration and minimal contact resistance between the pillars the total length of the multilayer was varied between 1400Å and 2800Å and the GMR-effect was measured. In e-beam evaporated Co/Cu

multilayers an optimum is reached with a multilayer length of 2200. The path of these electrons is shown in figure 3.2. To get a better idea of the real shape of the multilayers, SEM (Scanning Electron Microscopy) pictures are taken. In figure 3.3 a SEM picture is shown of a Fe/Cr multilayer. In this figure the substrate and the pillars are both visible. Because the length of the pillars is much larger then 0.17 μm, the ideal current path is different from the one shown in figure 3.2.

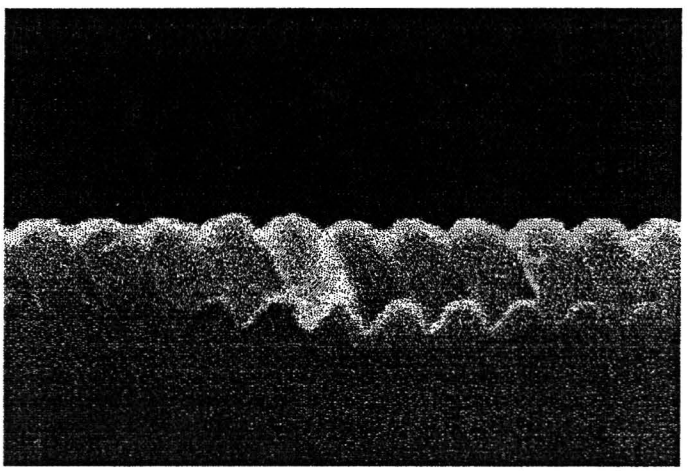

Figure 3.3. *SEM picture of a multilayer grown on a grooved substrate. The multilayerlength is larger than the groovelength. The current path will be different form the ideal current path shown in figure 3.2.*

The total size of the grown sample is approximately 5 x 10 mm. In order to do both CIP and CPP measurements the sample has to be kleeved into smaller parts of approximately 1 x 4 mm. Now the samples are attached to a chipcarrier. The contacts with the chipcarrier are made with thin aluminium wires. These wires are ultrasonically bonded into both sample and chip-holder. Four contacts are made because the GMR measurements are done in the four probe measuring geometry. The sample is now ready for measurement. The result is shown in figure 3.5. because of the rectangular shape of the sample the current distribution is well defined. To compare the resistances of the different samples, the measured resistances were corrected for their geometry. Therefore the precise geometry was determined with a microscope to 0.10 mm exactly.

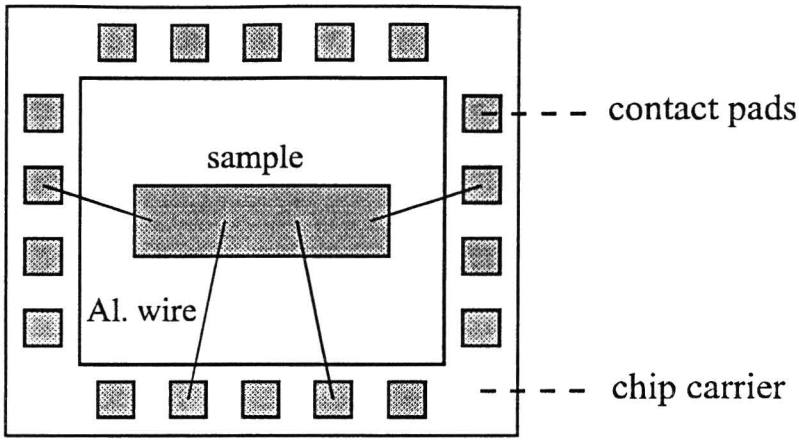

Figure 3.4. Schematic view of the sample on the chipcarrier.

3.3 Sample characterisation.

The structure of the interface is an important aspect of the GMR-effect. For example the magnetic moments of the impurities located at the interface are important for spin dependent scattering where the number of impurities is important for the interface resistance. To characterise this microstructure, two methods are used. Magnetisation measurements with a VSM (Vibrating Sample Magnetisation) are done to examine the magnetic behaviour of the magnetic moments and X-ray diffraction measurements are done to examine the microstructure of the multilayer. Both methods are described below.

3.3.1 VSM measurements.

The magnetisation of the samples was measured using a vibrating sample magnetometer or VSM. A schematic picture of the VSM set-up is shown in figure 3.5.. The principle of the VSM is to vibrate the sample with a frequency of approximately 80 Hz. The magnetisation of the sample is induced by a homogeneous magnetic field varying from -1300 to 1300 kA/m.

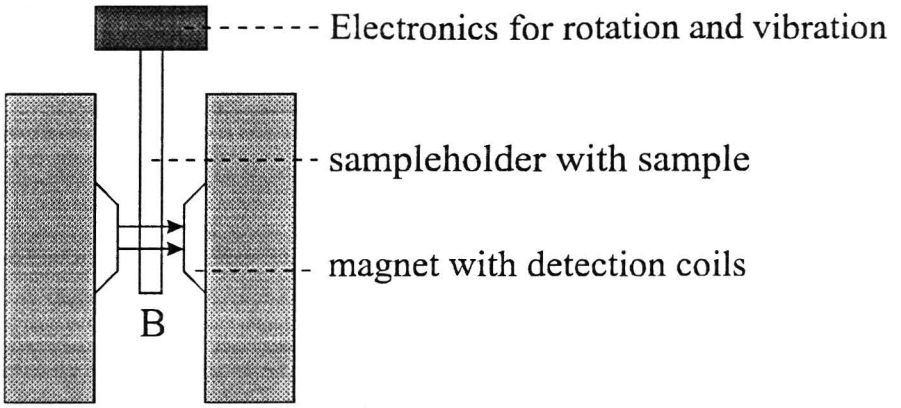

Figure 3.5. *Schematic picture of the VSM set-up.*

The magnetisation in the vibrating sample causes an induced voltage in four pick-up coils around the sample. With the use of four coils it is possible to measure the magnetisation parallel and perpendicular to the applied field in one time. Now the magnetisation is measured as a function of the magnetic field varying for $-H_{max}$ to H_{max} and back. This is the so called magnetisation curve. With this magnetisation curve the easy axis of the magnetisation and the saturation magnetisation can be determined. When the bulk value for the magnetisation and the total volume of magnetic material are known, the total magnetisation van be calculated. When the measured value of magnetisation is lower than the calculated one, we can determine the effective magnetic dead layerthickness by assuming that this difference is caused by changed magnetic moments at the interfaces. This leads to an expression for the effective dead magnetic layer, which is:

$$M_s = \frac{m_s}{A} \frac{1}{t_m - t_{dead}} \qquad (3\text{-}1)$$

where M_s is the value for bulk magnetisation, m_s the measured magnetic moment, At_m the total volume of the magnetic material and t_{dead} the total effective magnetic dead layerthickness of the multilayer

3.3.2 X-ray diffraction.

A Powerful tool to examine the structure of a sample is x-ray diffraction (XRD). This technique can be used to examine periodic structures and is therefore often used in solid state physics. The method is based on the well known Bragg reflection. A schematic view is shown in figure 3.6.

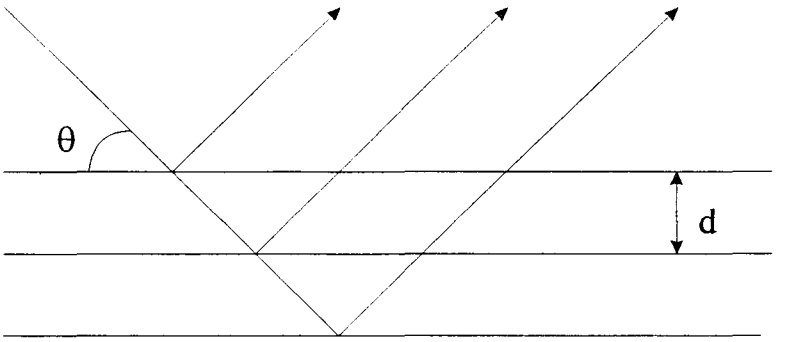

Figure 3.6. *Schematic view of Bragg reflection. At every interface a part of the incoming beam is reflected.*

In normal crystals, Bragg reflection occurs when the wavelength of the x-ray fits the period of the crystal. This means that Bragg reflection occurs at an angle θ for which:

$$2d\sin\theta = k\lambda \tag{3-2}$$

where d is the length of the period in the crystal and λ the wavelength of the x-ray. In a multilayer there are three periods: the multilayer period D and the periodicities for the two crystalline layers d_A and d_B of layers A and B. Segmuller and Blakeslee [20] showed that the resulting diffraction pattern consists of sets of peaks at positions centred around the Bragg positions at which peaks would have occurred for the separate materials A an B. These are the so called satellite peaks. From this diffraction pattern the multilayer period can be determined with:

$$\Lambda = \frac{m\lambda}{2(\sin\theta - \sin\langle\theta\rangle)} \tag{3-3}$$

The number of satellites is dependent of the structure of the multilayer. When the interfaces are very rough, no satellites will be visible.

3.4 Magnetoresistance measurements.

All transport properties were measured in a four-probe measuring geometry. Because voltage and current leads are separated, all possible effects of lead resistance are excluded. When both voltage drop and current are known, the resistance can be determined. Before preparation on the chip carrier takes place, the resistance of all samples is checked with a simple four-probe measurement set-up.

The magnetoresistance measurements which are used for the results in chapter 4, are performed with the set-up shown in figure 3.7. The set up can be devided in two parts. One part for measuring and data acquisition and one part for temperature control.

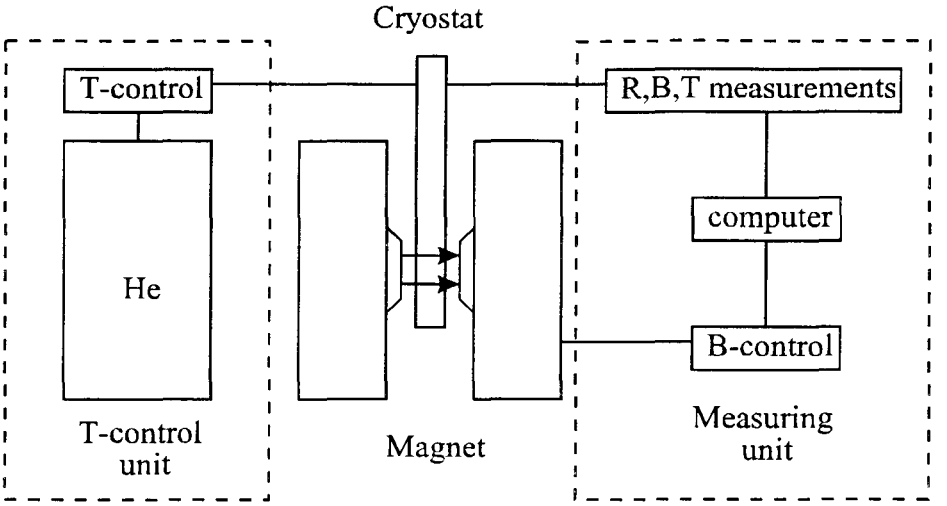

Figure 3.7. *Schematic view of the GMR measuring set-up. R, T and B are the resistance, temperature and magnetic field respectively .*

The resistance is measured with a Linear Research LR-400 resistance bridge. The maximum resistance to be measured can be set from 20 mΩ to 200 kΩ. The accuracy can be improved by subtracting an offset. In this way an accuracy of 0.01% can be reached. The current used during the experiments is 1 mA. The temperature is measured with a Pt resistance in the cryostat. This resistance is calibrated in range from 80-373 K. The magnetic field is measured with a Hall probe. The magnetic field was applied by two water cooled copper coils with a maximum field of 2T (by a current of 50 A). The magnetic field is controlled with a steering voltage to the magnet power supply. This voltage is applied by a HP function generator and the frequency used was approximately 0.001 Hz. The total measuring time is between 15 and 30 minutes.

In order to carry out temperature dependent measurements, it is necessary that the temperature of the sample can be regulated. Therefore the sample is placed in a cryostat which is connected to liquid helium. The flow of the helium through the cryostat is regulated by a Oxford He-flow control and has to be set manually. For regulation of the temperature a PID (Proportional, Integrate, Differentiate) controller is used. This controller is attached to a temperature sensor and a heating element both in the cryostat.

4. Results and discussion.

The GMR-effect is measured in Co/Cu, Cu/Ru, Fe/V and Fe/Cr multilayers with varying nonmagnetic layerthicknesses. The results of these measurements are described and discussed. Magnetisation measurements are done in order to examine the magnetic properties of the multilayers. These measurements can be used to investigate the existence of a magnetic dead layer caused by reduced magnetic moments located at the interface. The crystal structure is examined with x-ray diffraction.

4.1 Co/Cu multilayers.

In this paragraph the results of measurements of Co/Cu multilayers grown on grooved substrates are given. The first multilayers on grooved substrates have been grown in a MBE system. The Co/Cu multilayers showed a difference in GMR-effect between the CIP- and the CPP-configuration (CPP/CIP≈4) indicating that the technique of grooved substrates is very powerful to examine the GMR-effect in the CPP-configuration. The multilayers used in the present research have been grown by e-beam evaporation. In figure 4.1 the measured GMR-effect of these samples is compared with the MBE grown samples. For both methods it is clear that there is a difference between the GMR-effect in the CIP- and the CPP-configuration.

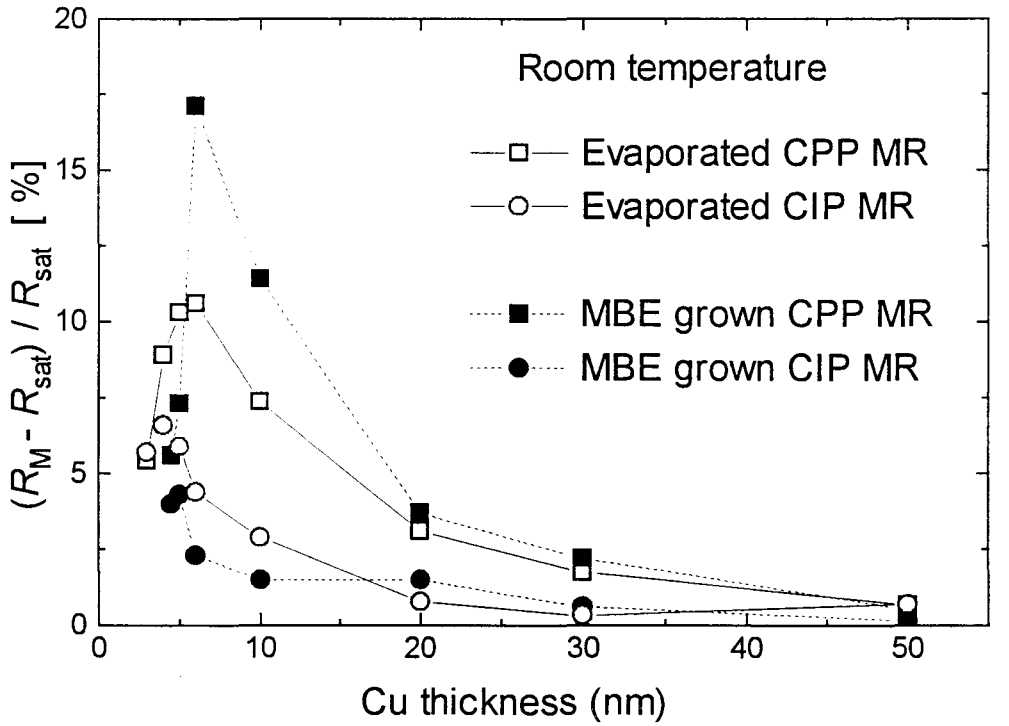

Figure 4.1. The GMR-effect of the two differently grown series of multilayers with a Co layerthickness of 15Å. Measurements are done in both CIP- and CPP-configuration.

The maximum GMR-effect in the MBE grown multilayers is 17% and is reached in the CPP-configuration with a Cu layerthickness of 60Å. Below this Cu layerthickness the GMR-effect is rapidly decreased. This can be explained by the existence of pinholes in the thin Cu layers, by which the Co layers are magnetically connected. In the e-beam evaporated multilayers a maximum of 11% is reached in the CPP-configuration with a Cu layerthickness of 60Å. Like in the MBE grown multilayers the GMR-effect is decreased with smaller Cu layerthickness. In the e-beam evaporated multilayers, the GMR-effect in the CIP-configuration is higher compared to the MBE grown multilayers. From GMR measurements in multilayers with varying Co and Cu layerthicknesses, the bulk Co ,bulk Cu and interface resistance, together with the spin asymmetry parameters β and γ for bulk and interface respectively, are determined using the two channel model described in chapter 2. These values are shown in table 4.1

Table 4.1. *The spin-dependent scattering parameters at 4.2K for Co/Cu multilayers [21].*

	AR ($f\Omega m^2$)	β	γ	ρ_{Co} ($\mu\Omega cm$)	ρ_{Cu} ($\mu\Omega cm$)
MBE	0.20±0.04	0.17±0.03	0.45±0.09	4.1±0.7	0.39±0.07
e-beam	0.41±0.07	0.25±0.03	0.26±0.07	6.6±0.6	1.3±0.4

The interface resistance of e-beam evaporated multilayers is about twice as high as of the MBE grown multilayers. Because the interface spin asymmetry parameter is about half the MBE value, it is clear that the increase in interface resistance originates from spin independent scattering. Probably, this difference is caused by the less vacuum quality of the e-beam evaporation set-up.

These measurements show that it is possible to use e-beam evaporated multilayers to examine the GMR-effect in the CPP-configuration. In the following paragraphs the results of GMR-measurements done with other materials given

4.2 Co/Ru multilayers.

The samples used in these measurements all have a Co layerthickness of 15 Å. The Ru layerthicknesses are 30Å, 60Å, 100Å and 200Å. The GMR-effect is measured in both CIP- and CPP-configuration. The multilayers were grown on grooved substrates.

First we look at the CIP-configuration. The resistance of the multilayers of the multilayers is measured between 4.2 K and room temperature (293 K). The resistances of the CIP-configuration at 4.2K and at room temperature are shown in figure 4.2. Except for the 200Å Ru multilayer the resistance is decreasing with increasing Ru layerthickness. This decrease of the resistance is caused by the decreasing influence of interface scattering. When the mean free path of the electrons becomes much smaller than the layerthickness, the influence of interface scattering is negligible. From these measurements it is very difficult to determine the mean free

path of the electrons in the Ru layers. The difference in resistance between the two temperatures is very small.

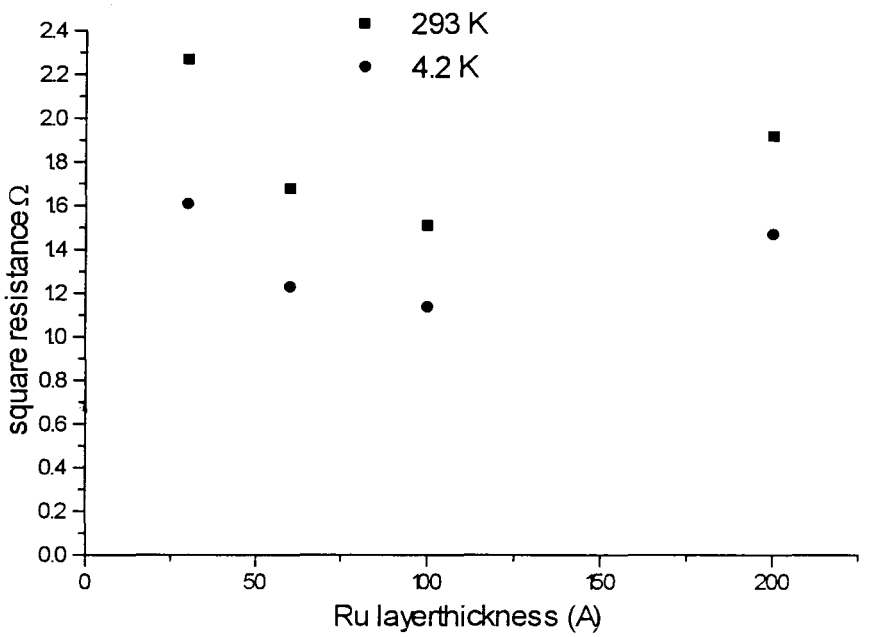

Figure 4.2. *Resistance of the Co/Ru multilayers in the CIP-configuration as a function of the Ruthenium thickness.*

In figure 4.3 the results of GMR measurements in the CIP-configuration of the Co/Ru multilayers is given as a function of the Ru layerthickness. The measurements were done at 4.2 K and at 293 K. The maximum GMR of 0.22% is found in the 30 Å Ru multilayer at 4.2 K. This is in good agreement with other experimental results of other groups. Dinia and Ounadjela [12] found a value of 0.38% for a Co/Ru sandwich (two bilayers) with a Ru layerthickness of 6Å. Bloemen [22] found a maximum of 0.09% for a Co/Ru multilayer with a Ru layerthickness of 16Å. The latter was measured at room temperature.

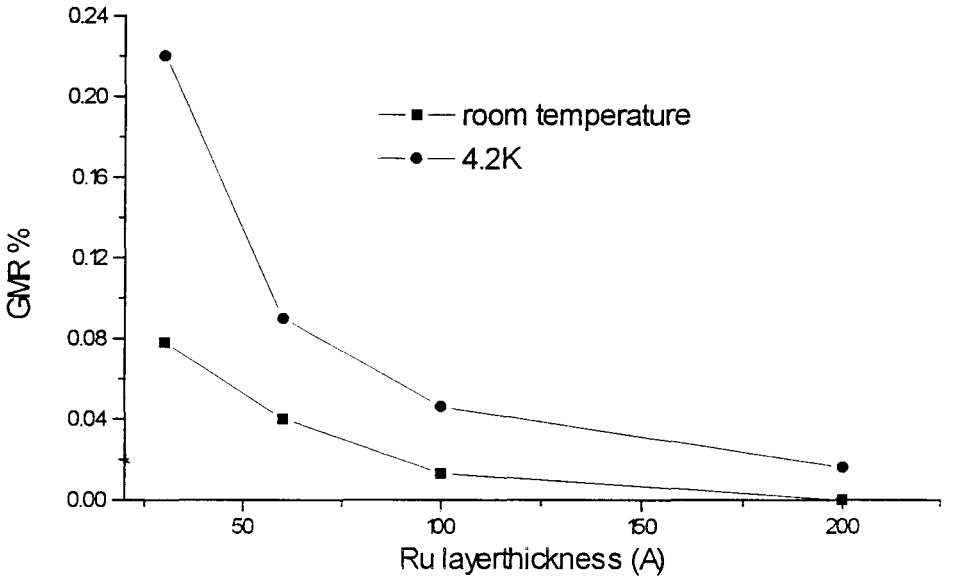

Figure 4.3. *Giant magnetoresistance of Co-Ru multilayers in the CIP-configuration as a function of the Ru layerthickness*

With increasing Ru layerthickness the GMR-effect becomes smaller. The amount of spin dependent scattering is decreasing. In addition to this, the mean free path of the conduction electrons becomes small compared to the Ru layerthickness. This also leads to a decrease in GMR-effect. The GMR-effect at 4.2 K is about three times the value at room temperature. In the resistance there is not much difference between these two temperatures. The difference in GMR-effect can therefore not be explained with an additional spin independent resistance due to, for instance, electron-phonon scattering.

The GMR-effect is also measured in the CPP-configuration. In figure 4.4 the resistance of the multilayers in the CPP-configuration is shown. Except for the 200Å Ru multilayer, the resistance is increasing with increasing number of bilayers. Assuming that the difference between the Co and Ru resistances is small compared with the total resistance, the slope is equal to the interface resistance.

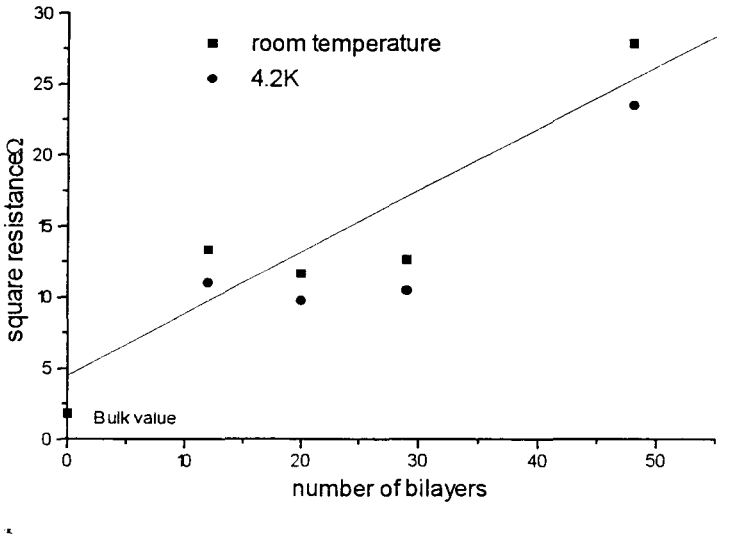

Figure 4.4. The resistance of Co/Ru multilayers in the CPP-configuration as a function of the Ru layerthickness.

The square resistance is about 10 times higher compared with the CIP-configuration. This means that almost all the resistance originates from interface scattering or from resistance caused by the connection of the separate multilayers, the contact resistance. When the number of bilayers is zero, all the resistance is caused by bulk scattering and is approximately equal to the CIP-configuration (assuming that the contact resistance and the difference between the bulk Co and the bulk Ru resistances is very small compared to the interface resistance). This value is shown in figure 4.3 as the bulk value for the resistance. The interface resistance is approximately 8.6 ± 3 fΩm^2 and has little dependence on the temperature. This is about 20 times higher as the interface resistance in e-beam evaporated Co/Cu multilayers also grown on grooved substrates. Part of this can be understood from the 8% lattice mismatch in Co/Ru interfaces causing dislocations in the interface. Up to know, no other experimental values of the Co/Ru interface resistance are known.

The results of GMR measurements are shown in figure 4.5. As in the CIP-configuration, the values of GMR are very low. A maximum of 0.27% is reached in the 30Å Ru multilayer at 4.2K. This is only little more as in the CIP-configuration. Because almost all the resistance originates from interface scattering, it is clear that this scattering is very much spin independent in contrast to Ru impurities in Co.

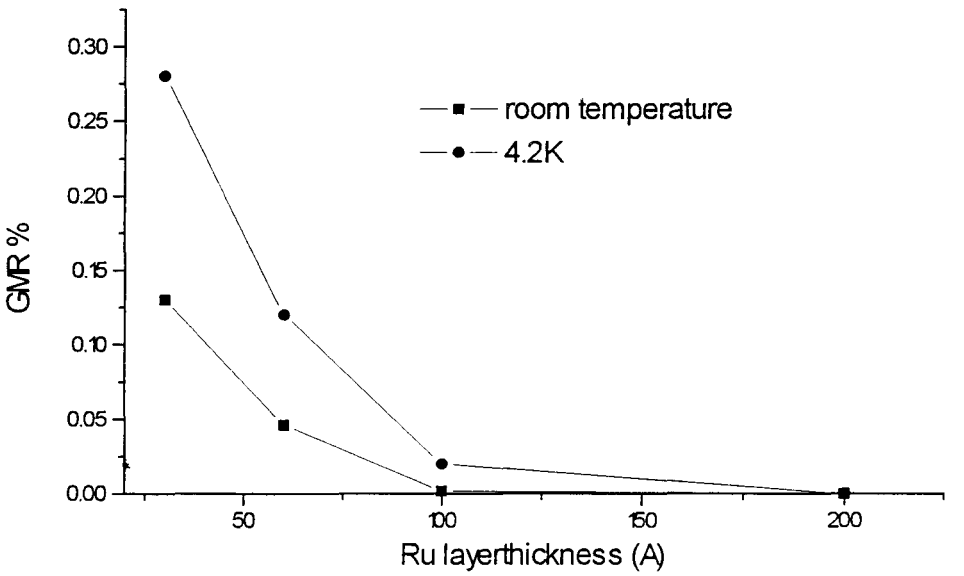

Figure 4.5. *GMR-effect of Co/Ru multilayers in the CPP-configuration as a function of the Ru layerthickness.*

Unlike in the CIP-configuration, we did not found a GMR-effect in the 200Å Ru multilayer. The reason for this could be that the spin-flip diffusion length in Co/Ru multilayers is very small. From the Boltzmann model in the CPP-configuration it is clear that the GMR vanishes when the spin-flip diffusion length becomes small compared to the layerthickness. To determine this spin-flip diffusion length, $A\sqrt{(R_{AP}-R_P)R_{AP}}$ is plotted in figure 4.6 as a function of the number of bilayers and compared with results from the Boltzmann model (equations (2.19) - (2.22)).

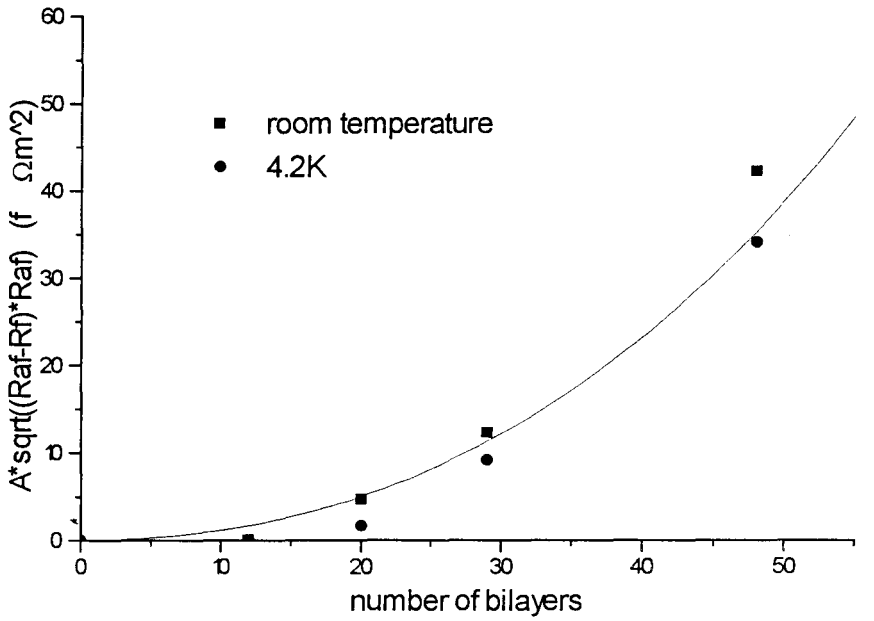

Figure 4.6. *$A\sqrt{(R_{AP}-R_P)R_{AP}}$ as a function of the number of bilayers. In the absence of spin-flip scattering a straight line through the origin is expected.*

The best fit is found for a spin-flip diffusion length of 30Å and a interface scattering asymmetry parameter γ of 0.1. The bulk spin asymmetry parameter β is taken at 0.15 as is found in e-beam evaporated Co/Cu multilayers grown on grooved substrates, but in Co/Ru multilayers this value does not have much influence on the GMR because of the strong interface scattering. The resistance for bulk Co and bulk Ru is taken at 50μΩcm, the value of CIP- resistivity. Again, these values do not have much influence on the total resistance. The interface resistance is taken at 8.6 fΩm^2 as determined from the CPP resistance.

To determine the magnetic properties of the Co-Ru multilayers, magnetisation measurements are done. The magnetisation is measured parallel (x) and perpendicular (y) to the applied field and with the applied field parallel (top) and perpendicular (bottom) to the plane of the layers. The magnetisation curves of a 15Å Co 30Å Ru are shown in figure 4.7.

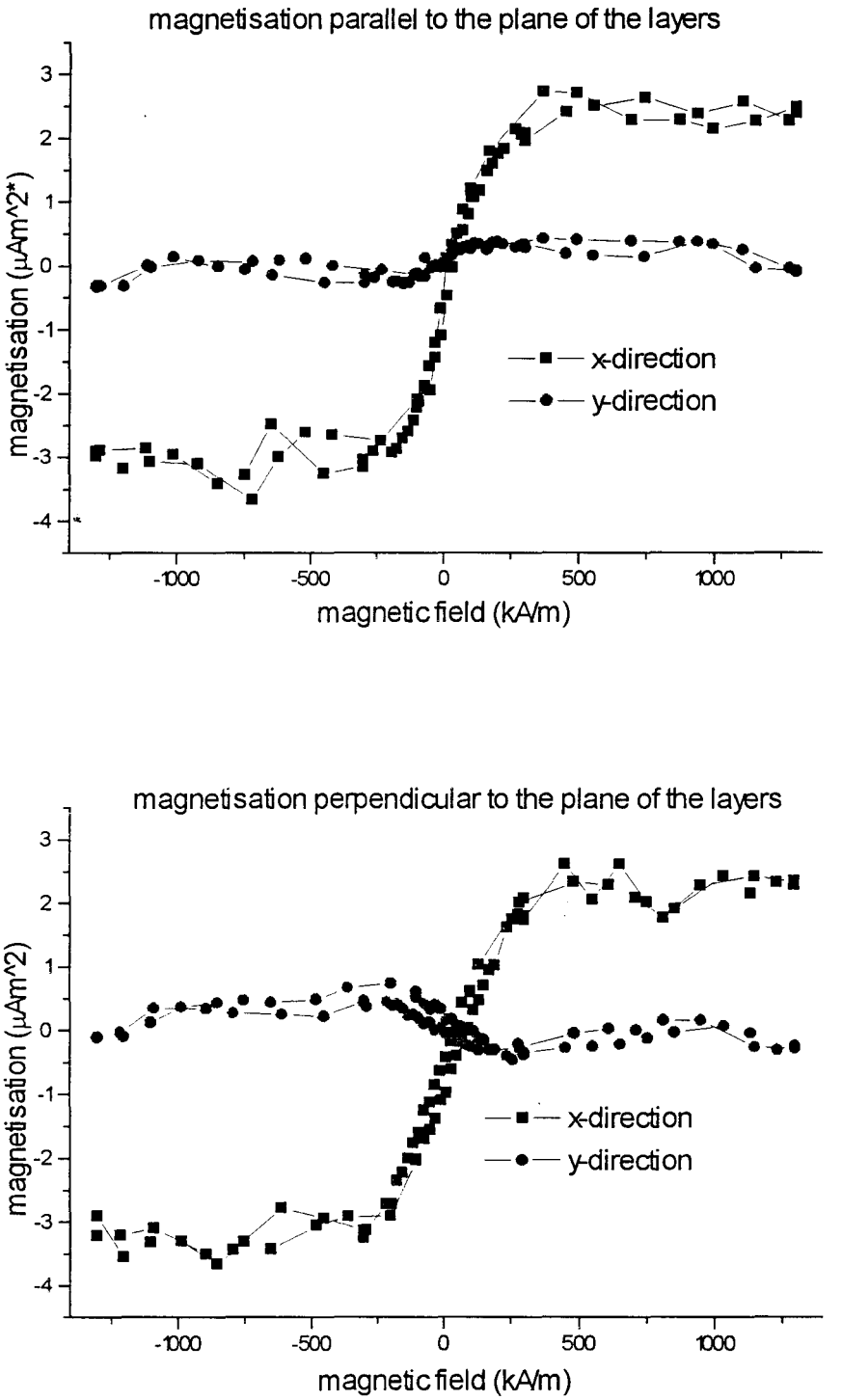

Figure 4.7. *Magnetisation curves for a 15Å Cobalt 30Å Ruthenium multilayer. The magnetisation is measured parallel (x) and perpendicular (y)to the applied field and with the magnetic field parallel (top) and perpendicular (bottom) to the plane of the layers. The measurements are done with multilayers grown on flat Si substrates.*

Due to shape anisotropy the easy axis of the magnetisation is in the plane of the layers. But the difference between the saturation magnetic fields perpendicular and parallel to the layers is very small. Daalderop* calculated that for a single Co layer the easy axis is perpendicular to the layer. Probably, the 15Å Ru multilayer is an intermediate situation between parallel and perpendicular magnetisation. From these measurements the saturation magnetisation can be determined and compared to the literature M_s of bulk Co ($1.43\ 10^6$ kA/m). When we assume that the difference between the measured and the calculated values is caused by the magnetic moments located at the interface, an effective magnetic dead layerthickness can be calculated. A value of approximately 2Å is found. This means that the number of d-electrons in atoms located at the interface is changed with respect to bulk impurities. The scattering asymmetry parameter α=0.22 for Ru impurities in Co [12] is no longer a good indication for spin dependent interface scattering. Probably, a thin layer of nonmagnetic CoRu alloy gives rise to spin independent interface scattering decreasing the size of the GMR-effect. Due to the high value of interface resistance, the spin dependent scattering originating from bulk Co is completely overshadowed. Additional spin-flip scattering further decreases the GMR-effect.

4.3 Fe/V multilayers.

In figure 4.8 the resistance of Fe/V multilayers in CPP-configuration is shown as a function of the V layerthickness. Like in the Co/Ru multilayers the resistance in the CPP-configuration is about ten times higher as in the CIP-configuration. The absolute values of the resistance are also similar. From the resistance in the CPP-configuration the interface resistance can be determined and a value of 8.8 ± 3 fΩm^2 is found. Like in the Co/Ru multilayers, the bulk value for the resistance is taken as the resistance in the CIP-configuration.

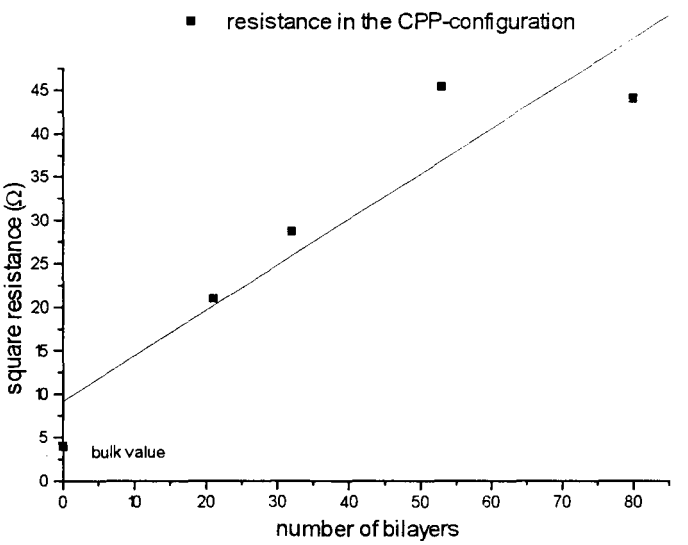

Figure 4.8. *Resistance of the Fe/V multilayer in the CPP-configuration as a function of the V layerthickness.*

In figure 4.9 the GMR values for the Fe-V multilayers in both CIP- and CPP-configuration is shown as a function of the V layerthickness. The measurements are done at room temperature. A maximum of 0.25% is reached in the 15Å V multilayer in the CPP-configuration.

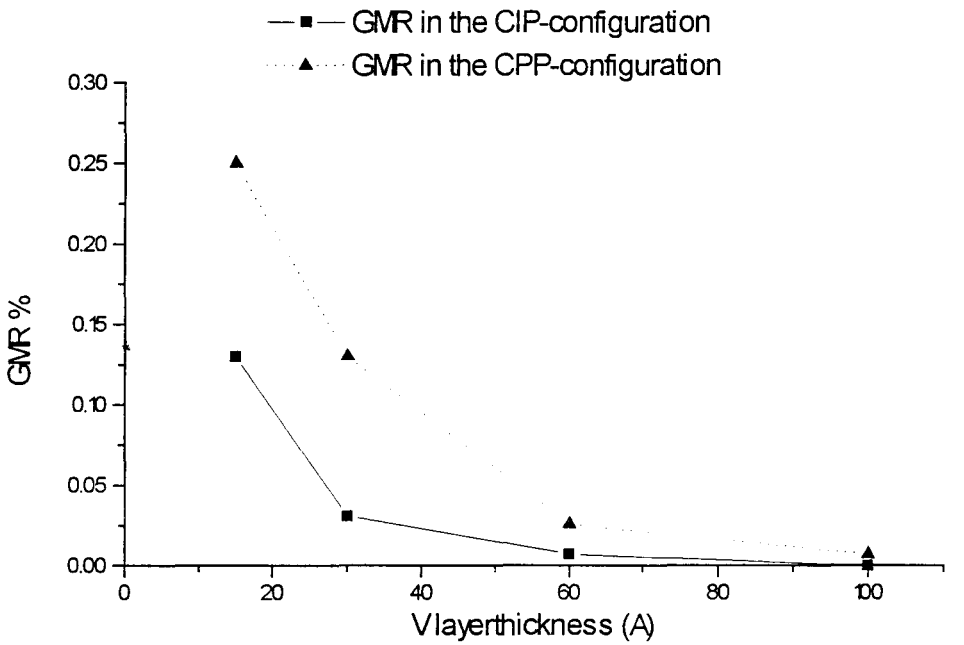

figure 4.9. *GMR in both CIP- and CPP-configuration as a function of the V layerthickness. These measurements are done at room temperature.*

The GMR values in the CPP-configuration are about twice as high as in the CIP-configuration where in the Co/Ru multilayers they were approximately the same. Because in the CPP-configuration almost all the resistance originates from interface scattering, this scattering is very much spin independent. Again, like in the Co/Ru multilayers, the spin asymmetry parameter for V impurities in Fe is no longer a good indication for spin dependent interface scattering. To determine the spin-flip diffusion length in the Fe/V multilayers, $\sqrt{(R_{AP}-R_P)R_{AP}}$ is plotted as a function of the number of bilayers. The result is shown in figure 4.10. It is not possible to make a linear fit through the origin. This means that the spin-flip diffusion length is not large compared to both layerthicknesses. The solid line in figure 4.10 is a fit made with a spin-flip diffusion length of 50Å.

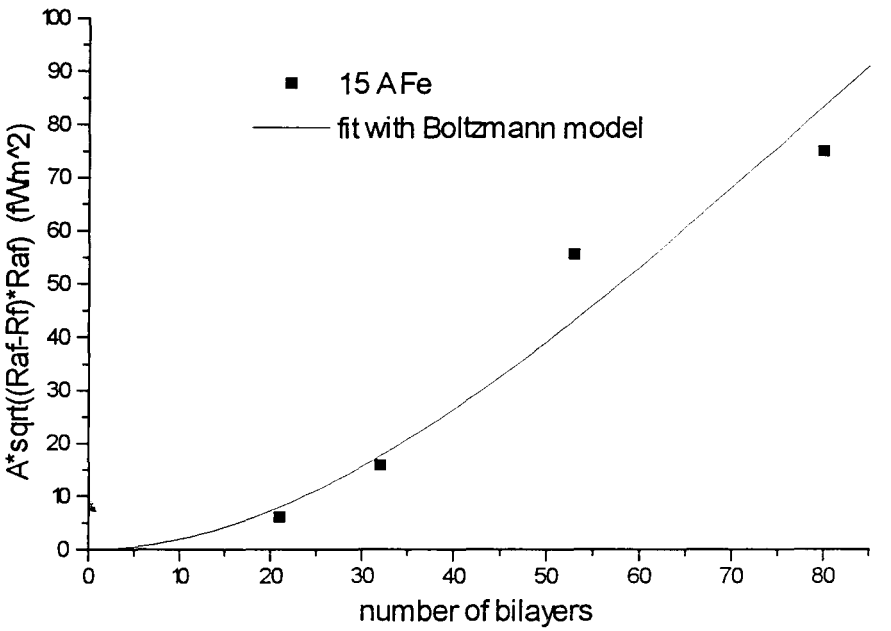

Figure 4.10. *$A\sqrt{(R_{AP}-R_P)R_{AP}}$ as a function of the number of bilayers. The solid line is a fit made with the Boltzmann model with a spin-flip diffusion length of 50Å.*

At 4.2K, GMR measurements are done with the 15Å V multilayers in the CPP-configuration. A value of 1.44% in reached. This is approximately 6 times the value at room temperature. The resistance is approximately the same. This means that the difference in GMR-effect is not caused by additional spin independent bulk resistivity. Probably, unlike in Co/Ru multilayers, the spin-flip diffusion length in Fe/V multilayers is dependent on the temperature.

To determine the magnetic properties of the Fe-V multilayers, magnetisation measurements are done. These magnetisation measurements are done with the magnetic field parallel (x) and perpendicular (y) to the layers. The results of these measurements are shown in figure 4.11.

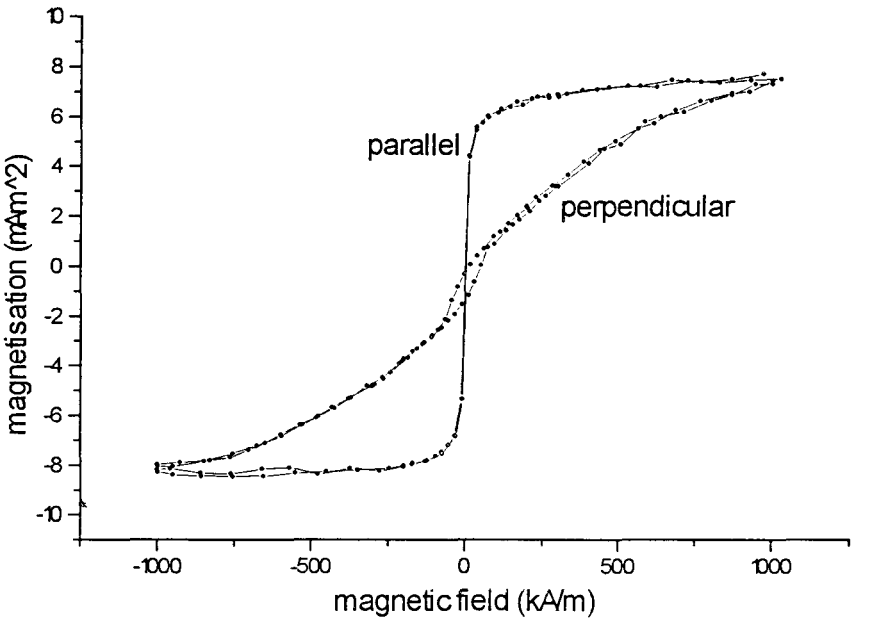

Figure 4.11. *Magnetisation curves of a 15Å V / 15Å Fe multilayer. These magnetisation measurements are done with the magnetic field parallel and perpendicular to the layers The magnetisation measurements are done with a multilayer grown on a flat Si substrate..*

The easy axis of the magnetisation is in the plane of the layers due to shape anisotropy. From this measurement the saturation magnetisation can be determined and compared with the literature value of bulk Fe (1.73 kA/m). When we assume that the difference between the measured and the calculated values is caused by the magnetic moments located at the interface, an effective dead magnetic layerthickness can be calculated and a value of 2Å is found.

In chapter 2 the influence of the magnetic moments on the spin dependent scattering is discussed. A large asymmetry is expected from the bulk values of d-electrons and from measurements done with V impurities in Fe [11]. In a magnetic dead layer there are no magnetic moments and therefore the scattering is spin independent. Like in Co/Ru multilayers, the spin dependent scattering in bulk Fe is completely overshadowed by the strong spin independent interface scattering. The GMR-effect is further decreased by spin-flip diffusion length of 50Å.

4.4 Fe/Cr multilayers.

The results of GMR measurements of Fe/Cr multilayers shown in figure 4.12. These measurements are done at room temperature. A maximum of 3.2% is reached in the 15Å Chromium multilayer at room temperature. These values are similar to the ones found by the

group of Gijs in microstructured multilayer pillars [4]. They measured a GMR of approximately 1% in the CPP-configuration and 0.5% in the CIP-configuration for a 30Å Fe / 40Å Cr multilayer at room temperature. But, in a 30Å Fe / 10Å Cr they measured a GMR-effect of approximately 20% at room temperature, increasing to 110% at 4.2K

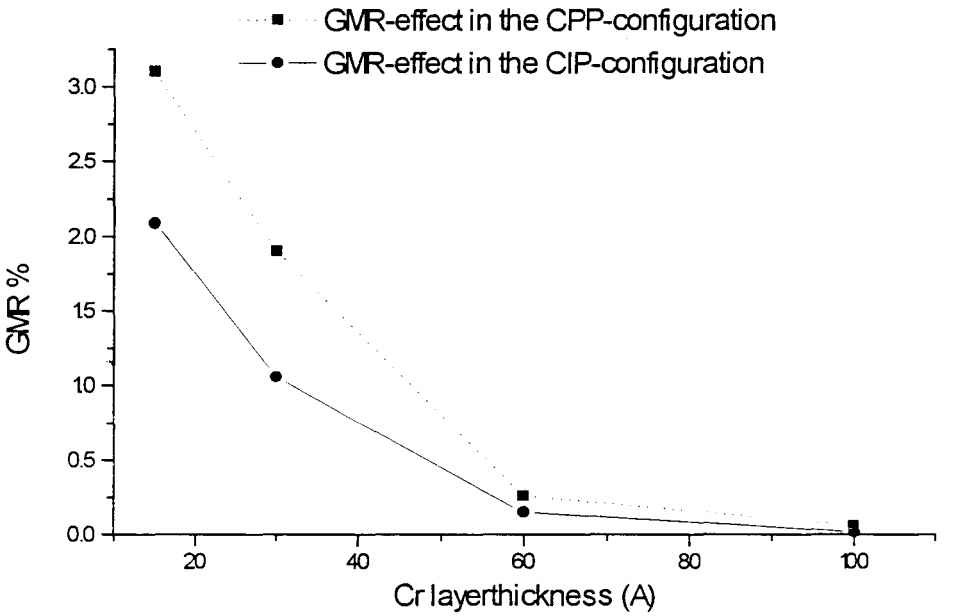

Figure 4.12. *GMR in Fe/Cr multilayers as a function of the Cr layerthickness. These measurements are done at room temperature.*

The GMR-effect is about ten times higher compared with Fe/V multilayers, while the resistance is similar to both Fe/V and Co/Ru multilayers. At 4.2 K, a GMR-effect of 10% is reached in the 15Å Cr multilayer in the CPP-configuration. This is approximately 3 times higher compared with room temperature. The Fe/Cr multilayers were grown with different growth rates for different Cr layerthicknesses and the resistances of the multilayers in the CPP-configuration ware decreasing with increasing number of bilayers (opposite as expected). To determine the influence of this growing rate on the resistance and the GMR-effect, a serie of 15Å Fe / 15Å Cr multilayers were grown with different rates varying from 1 to 10 Å/s. From these samples the resistance and GMR-effect is measured in both CIP- and CPP-configuration. The results are shown in figure 4.13

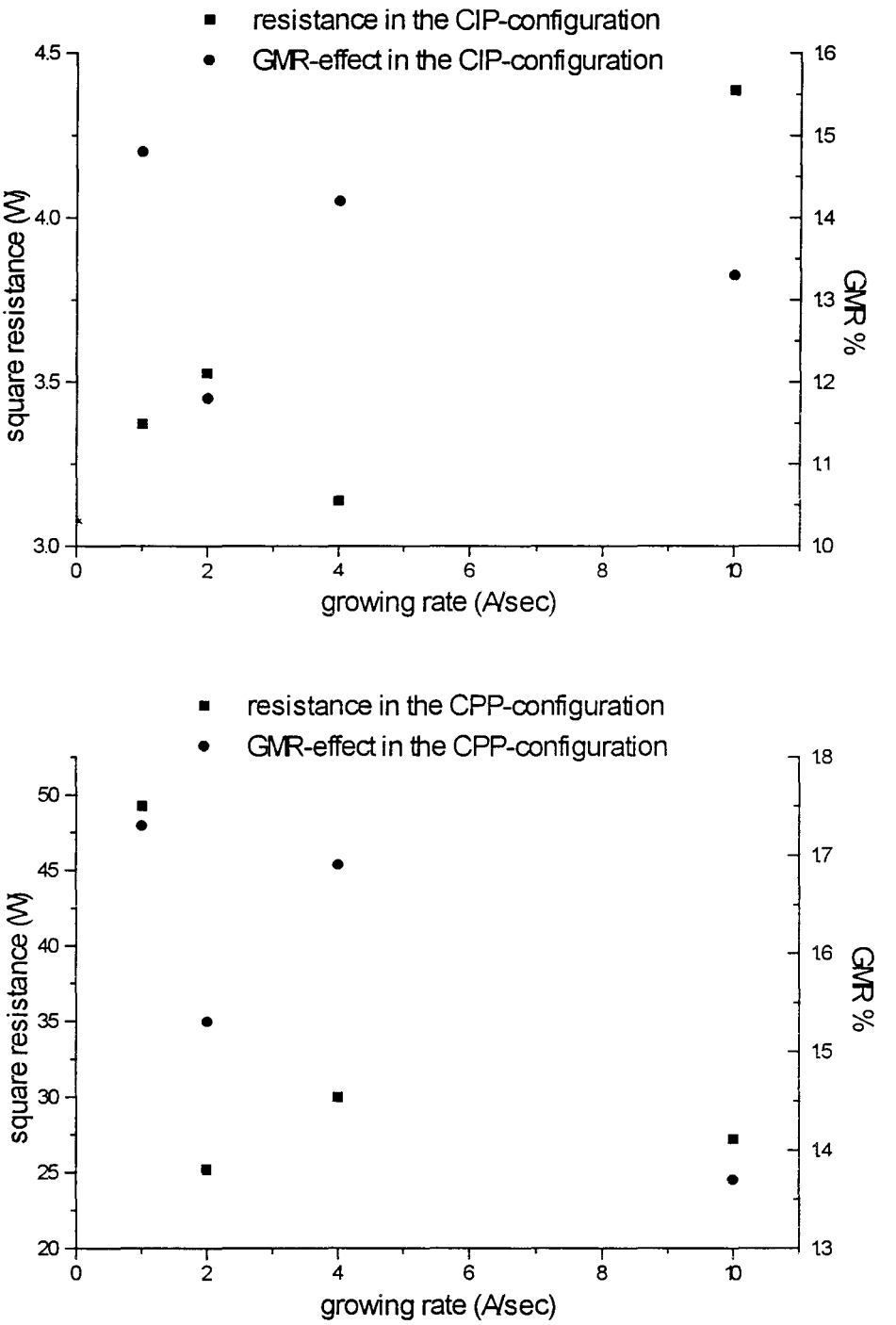

Figure 4.13. Resistance and GMR-effect in the CIP (top) and CPP (bottom) configuration as a function of the growing rate.

The values of GMR are all between one and two percent. A maximum of 1.73% is reached in the CPP-configuration and a maximum of 1.48% is reached in the CIP-configuration. This is below the values shown in figure 4.10. No clear dependence of both resistance and GMR-effect on the growing rate is found. For example the multilayer used in figure 4.12 is grown

with a growing rate of 3Å/sec. The resistance of this multilayer in the CPP-configuration is about 8Ω. The multilayer grown with a rate of 4Å/s has a resistance in the CPP-configuration of about 30Ω. This difference is very large while the growing rates are approximately the same. To further examine the origin of this difference, SEM pictures are made and shown in figure 4.14.

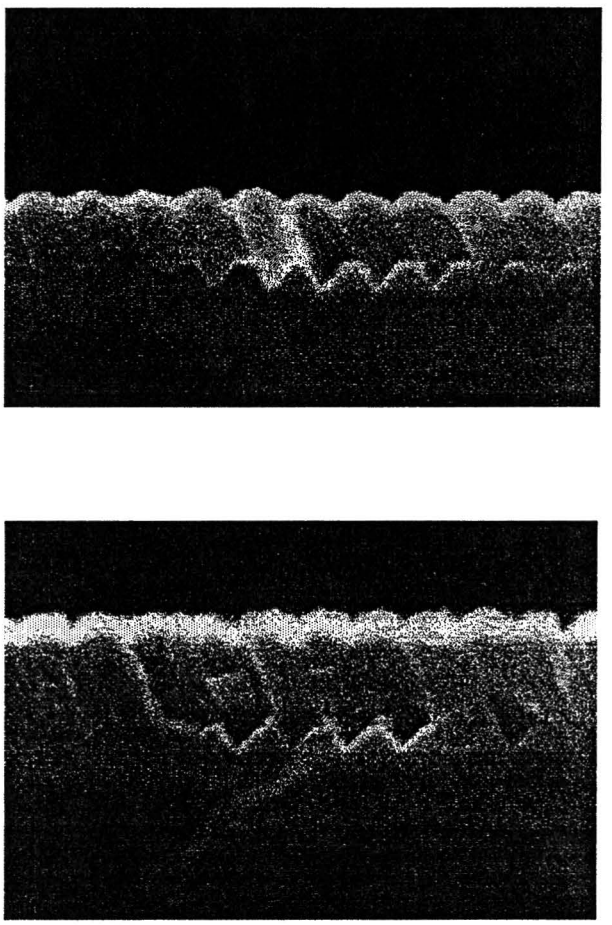

Figure 4.14. *SEM pictures of two 15Å Fe / 15Å Cr multilayers deposited with 3Å/s (bottom) and 4Å/s (top). There is a large difference in total multilayer length, probably causing the difference in resistance.*

There is a large difference in total multilayer length. When the total multilayer length is much longer than the length of the groove, the conduction electrons pass less interfaces compared to the case of optimal multilayer length. Therefore the resistance in decreased. This indicates that the fabrication of the multilayers is not yet fully under control.

5. Conclusions.

With the use of grooved substrates it is possible to examine the GMR-effect in the CPP-configuration. When multilayers of various layerthicknesses are grown, it is possible to get an indication of the spin asymmetry parameter for interface scattering and the spin-flip diffusion lengths.

In this research, the GMR-effect in Co/Cu, Co/Ru, Fe/Cr and Fe/V magnetic multilayers grown on grooved substrates has been investigated in both CIP- and CPP-configuration. From the results of these measurements it is clear that the spin asymmetry parameters for the scattering of electrons at bulk impurities is not a good indication for the size of the GMR-effect. For example, the spin asymmetry parameters of electron scattering at Cr impurities in Fe and V impurities in Fe are approximately the same, while the difference in the GMR-effect between the two systems is very large. Probably, this difference is caused by a change of the magnetic moments of the atoms located at the interfaces between the magnetic and the nonmagnetic materials with respect to the magnetic moments of impurities in the bulk of a material. The magnetic properties of Co/Ru and Fe/V multilayers are determined with magnetisation measurements and a magnetic dead layer is found of approximately 2Å, indicating a change in magnetic moments at the interface. From a simple model for scattering of free electrons at an impurity it can be understood that this magnetic moment is very important in spin dependent scattering. In Co/Ru and Fe/V multilayers, the GMR-effect is decreased by a small (approximately 40Å) spin-flip diffusion length.

Unfortunately, the fabrication of the multilayers is not yet fully under control. The length of the multilayers is different for the different multilayers as is shown with SEM-pictures of 15Å Fe / 15Å Cr multilayers grown with different growing rates.

Calculations show that the superlattice potential has an influence on the GMR-effect. But in the diffuse scattering regime, it is very difficult to determine the contribution of the superlattice potential to the GMR-effect. To determine this contribution, measurements have to be done in the ballistic transport regime. It could be interesting the determine the GMR-effect in Co/Ru multilayers in the ballistic regime because of the expected spin dependent potential steps at the interfaces between Co and Ru.

6. References.

[1] P. Grüngerg, R Scheiber, Y. Pang, U. Walz, M.B. Brodskey ans H.Sowers, J. Appl. Phys 61 (1987) 3750

[2] G. Binasch, P. Grünberg, F. Saurenbach and W. Zinn, Phys. Rev. B. 39 (1989) 2472

[3] W.P. Pratt, Jr., S.-F. Lee, J.M. Slaughter, R. Loloee, P.A. Schroeder andJ. Bass, Phys. Rev. Lett. 66 (1991) 3060

[4] M.A.M. Gijs, S.K.J. Lenczowski and J.B. Giesbers, Phys Rev Lett. 70 (1993) 3343

[5] P.M. Levy, S. Ẑhang, T. Ono and T. Shinjo, Phys Rev B. 52 (1995) 16049

[6] C. Kittel, Solid state physics, sixth edition, 1986

[7] S. Gasiorowicz, Quantum Physics, 1974

[8] C. Kittel, Quantumtheory of the solid state, chapter 18

[9] H. Itoh, J. Inoue and S. Meakawa, Phys. Rev. B. 47 (1993) 5809

[10] R. Coehoorn, J.M.M.M. 151 (1995) 341-354

[11] R. Coehoorn, J.M.M.M. 121 (1993) 432-435

[12]] A. Dinia and K. Ounadjela, J.M.M.M. 146 (1995) 66-76

[13] R. E. Camley and J. Barnás, Phys. Rev. Lett. 63 (1989) 664

[14] A. Fert, J.-L. Duvail and T. Valet, Phys. Rev. B, 52 (1995) 6513

[15] T. Valet and A. Fert, Phys. Rev. B, 48 (1993) 7099

[16] K. Schep, P. Kelly, G.E.W. Bauer, M.R.S. Symp. Proc. Vol. 384 305

[17] S. Zhang and P.M. Levy, M.R.S. Symp. Proc. Vol. 313 (1993) 53

[18] P. Bruno, J.M.M.M. 121 (1993) 248-252

[19] S.S.P. Parkin, Phys. Rev. Lett. 67 (1991) 3598

[20] A. Segmüller and A. E. Blakeslee, J. Appl. Cryst. 6 (1973) 19

[21] W. Oepts, M.A.M. Gijs, A. Reinders, R.M. Jungblut, J.M. Kerkhof, A.M.A. van Zon EMRS conference paper june 1996

[22] P.J.H Bloemen, Magnetic multilayers, Thesis EUT 1993

[23] G.E.O. Daalderop, Magnetic Anisotropy from First Principles, Thesis 1991

[24] P. M. Levy, Solid state physics, Advences in research and applications, volume 47 367

[25] M.A.M. Gijs and G.E.W Bauer, Perpendicular Giant Magnetoresistance of Magnetic Multilayers, to be published in 'Advances in Physics'

[26] J. Mathon, submitted to Phys. Rev. B. 1996

[27] R. van Gansewinkel, Graduation report, August 1995

7. Acknowledgements.

I would like to take this opportunuty to thank everyone at the Philips research laboratory who made my graduation period pleasant and informative.

-Wouter Oepts, my supervisor and the person I worked closest with.

-Wim de Jonge, for making this graduation project possible.

-Reinder Coehoorn and Martin Gijs, for suggestions and discussions.

-Jan Kerkhof, for growing the multilayers.

-Kees, Rene, Joost and Peter, for suggestions and discussions, and for plesant lunch and coffee breaks